Geological Quarterly, 2022, 66: 25
DOI: http://dx.doi.org/10.7306/gq.1657

Constraints on the nature and evolution of the volcanic fields of the Andahua Group, Central Volcanic Zone, southern Peru

Andrzej GAŁAŚ[1, *], Károly NÉMETH[2, 3, 4] and Paulina LEWIŃSKA[5, 6]

1 Polish Academy of Sciences, Mineral and Energy Economy Research Institute, Wybickiego 7A, 31-261 Kraków, Poland

2 Massey University, Volcanic Risk Solutions, School of Agriculture and Environment, Palmerston North, New Zealand

3 Institute of Earth Physics and Space Science, Sopron H-9400, Hungary

4 Saudi Geological Survey, Jeddah, Kingdom of Saudi Arabia

5 AGH University of Science and Technology, Faculty of Geo-Data Science, Geodesy and Environmental Engineering, Al. A. Mickiewicza 30, 30-059 Kraków, Poland

6 University of York, Department of Computer Science, Heslington, York YO10 5DD, Yorkshire, United Kingdom

Gałaś, A., Németh, K., Lewińska, P., 2022. Constraints on the nature and evolution of the volcanic fields of the Andahua Group, Central Volcanic Zone, southern Peru. Geological Quarterly, 66: 25, doi: 10.7306/gq.1657

The Andahua Group is a distinct cluster of typically monogenetic volcanoes located in the northernmost part of the Central Volcanic Zone in the Andes, characterized by small-volume lava domes and scoria cones. Seven volcanic clusters have been distinguished. Using satellite imagery, geological mapping, and fieldwork, we found a total of 103 lava domes, 43 scoria cones, and 3 small composite volcanoes. Most of the lava domes are monogenetic but 9 were formed by multiple eruptions. Petrogenetic models have been developed for the magma evolution of the Andahua Group. They show local crustal influence on the magmas generated, and possible controls on the magma pathway to the surface, and potential segregation. Local compositional variation of the crustal rocks is inferred to have a strong influence on the magma that ascends through the thick continental crust. Assimilation and contamination by deeply seated granitoids of the Arequipa and Paracas massifs are also inferred to play a role in the final magmatic products. Future activity with gas emissions from the Andahua Group volcanoes may cause hazardous conditions for tourists.

Key words: monogenetic volcanoes, small lava dome, petrological modelling, Andes.

INTRODUCTION

The western margin of South America is an active plate boundary where subduction of oceanic lithosphere beneath continental lithosphere has been occurring since the early Mesozoic (Mégard, 1987; Stern, 2004; Fig. 1A, B). Subduction in the so-called Central Volcanic Zone (CVZ) has been nearly continuous since 10 Ma (Somoza, 1998), producing a narrow present-day volcanic arc parallel with the plate boundary and some 230 km from it (England et al., 2004).

In the CVZ there are 44 composite volcanoes, 18 areas with small-volume, monogenetic-like, volcanic centres and 11 large silicic calderas (de Silva and Francis, 1991). In contrast to the well-studied large volcanoes, the small monogenetic volcanoes have received less attention. Many of these studies have been primarily focused on the morphometry of volcanic landforms or reconstruction of eruptive styles of individual volcanoes based on their eruptive products (Haag et al., 2019). However, interest among the research community of using the source to surface concept in understanding the evolution of these monogenetic volcanic fields has recently emerged (e.g., Gutiérrez et al., 2005; Guzmán et al., 2006; Cabrera and Caffe, 2009; Ureta et al., 2020). The small (in terms of eruptive volume) volcanoes, though, have received relatively limited attention. Good examples of such research in South America are investigations of small mafic and silicic volcanoes in Colombia (Borrero et al., 2017; Botero-Gómez et al., 2018; Murcia et al., 2019; Sánchez-Torres et al., 2019, 2022), research on several small-volume mafic to intermediate volcanoes in the CVZ in northern Chile (Ureta et al., 2019) and documentation of a few small, dispersed volcanoes in the Southern Volcanic Zone of Chile (Salas et al., 2017).

Recognition of the Andahua Group in Peru as a volcanic field is relatively recent (Delacour et al., 2007; Sørensen and Holm, 2008). This volcanic group is in the northern part of the CVZ (Fig. 1A), scattered across an area of 12,000 km^2. As many as 103 small lava domes and 43 scoria cones have been described during field research conducted between 2003 and 2017, aided by satellite image analysis (Gałaś, 2011, 2013). By comparison with the composite volcanoes, the Andahua Group

* Corresponding author, e-mail: agalas@min-pan.krakow.pl

Received: February 21, 2022; accepted: July 7, 2022; first published online: September 28, 2022

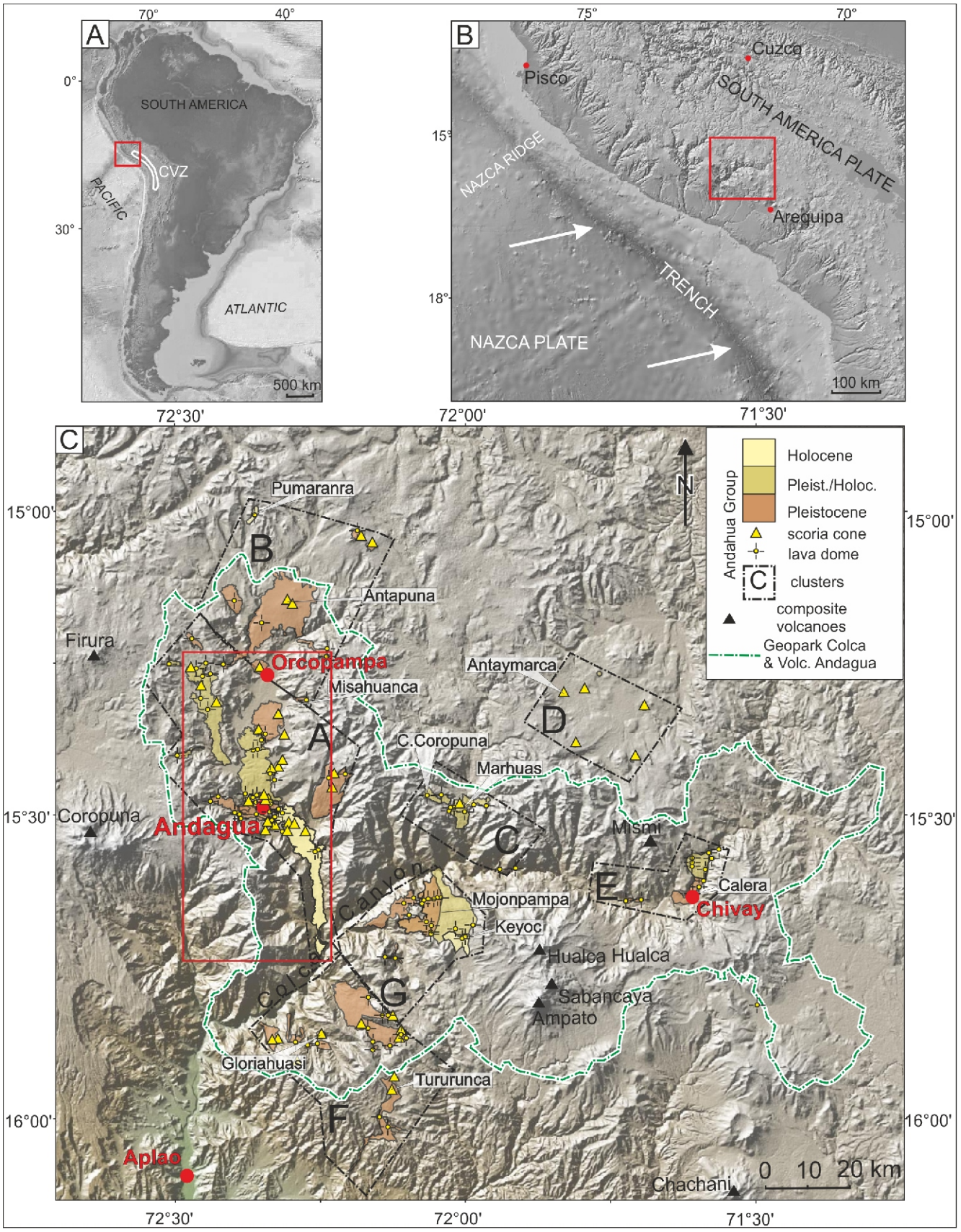

Fig. 1A – location of the Central Volcanic Zone in South America (CVZ); B – general tectonic context and research area, the red rectangle is the zoom shown in (C); C – Global Multi-Resolution Topography image showing distribution and age of the main volcanic and structural features of the Andahua Group and composite volcanoes in the region

The Andahua Group clusters have been grouped according to the bounding lineaments, relief, and tectonic settings: A – Valley of the Volcanoes, B – Antapuna, C – Río Molloco Valley, D – Lagoon Pariuhuana, E – Río Colca Valley, F – Pampa Jarán, G – Huambo-Cabanaconde; the red rectangle shows location of Figure 2

morphological forms are much simpler. Their volumes are typically within the range attributed to monogenetic volcanoes (<1 km^3). Geochemically, products of Andahua Group volcanoes are mainly intermediate (trachyandesite) as regards their silica content and correspond to the high-K calc-alkaline series (Delacour et al., 2007; Gałaś, 2014). The chemical range of the Andahua Group volcanic products shows some similarity to that of the widespread composite volcanoes in this region (e.g., SiO_2 wt.%: Andahua Group 52.8–67.8, Coropuna 55.5–71.7 – Venturelli et al., 1978; Hualca Hualca 55.8–63.1 – Mamani et al., 2010; Ampato 56.7–70.6 – Samaniego et al., 2016; see Fig. 1 for location of the volcanoes). The eruptive products in the CVZ mostly display high-K calc-alkaline andesitic and dacitic compositions. Petrological studies suggest that the underlying reasons for why minor volcanoes erupt in this part of the Andes are related to ascent through the crust without intercepting or developing large magma reservoirs (Wörner et al., 2018). Studies such as Mamani et al. (2010) and Delacour et al. (2007) provide information on two types of magma forming the Andahua Group. One of these (Delacour et al., 2007) was, most likely, modified by processes of assimilation by lower-crustal partial melts in the MASH (Melting, Assimilation, Storage, Homogenization) zone. These magmas on their way to the surface assimilated the Charcani Gneisses (from the Arequipa Massif) and other shallow crustal rocks (Delacour et al., 2007). The other magma type is related to two-component mixing and various fractional crystallization (FC) processes (Sørensen and Holm, 2008; Huang et al., 2017). The magmas of monogenetic centres, like the Andahua Group, display a primitive character (Wörner et al., 2018).

In this paper, we provide the first comprehensive summary of the volcanic fields of the Andahua Group from a source-to-surface perspective, with a general characterization of the 149 identified volcanoes. We: (1) provide physical volcanological descriptions of their eruptive products, (2) establish their relative chronology based on of fundamental volcano morphometry, also (3) provide petrographic and geochemical characterization of the volcanic products and (4) establish an overall evolutionary trend of the volcanoes. A better understanding of the magma regime of the scattered Andahua Group volcanoes can provide valuable information to help volcanic risk assessment.

GEOLOGICAL SETTING

The study area is located in the Central Andes in South America (Fig. 1A). The magmatic arc of the Central Andes is the result of convergence between the Nazca and South American plates, the former moving at a rate of ~9 cm/yr (Romanyuk, 2009) in a N80° direction (Sébrier and Soler, 1991, Fig. 1A, B). The continental crust in the central sector of the Central Andes displays the greatest thickness (up to 70 km) along the entire plate boundary (Beck et al., 1996). The Central Andean orocline has been active since the Jurassic Period with a culmination of volcanic eruptions from the Miocene (e.g., Thorpe et al., 1984; Trumbull et al., 1999). The magmatic arc has moved from the north-east to the south-west several times, in turn changing the composition (Mamani et al., 2010). Today the active CVZ arc is 2000 km long (England et al., 2004).

Magma in the Central Volcanic Zone (14–27°S, CVZ) displays a composition that is strongly affected by interaction with crustal material (Klerxs et al., 1979; Kay et al., 2005; Mamani et al., 2010, Godoy et al., 2014; Rivera et al., 2017). The mantle-derived magmas assimilated 20–40 vol.% of crustal rocks (Trumbull et al., 1999; Mamani et al., 2010). However, for the Quaternary magmas, the crustal contamination was estimated to be less significant – at 7–18 vol.% (Mamani et al., 2010). It is generally accepted that the CVZ magmas evolved by a range of possible processes such as: (1) assimilation-fractional crystallization (AFC), (2) fractional crystallization (FC), and (3) magma mixing (DePaolo, 1981; Gerbe and Thouret, 2004; Tepley et al., 2013). The processes of MASH are also thought to have been important for magma evolution (Delph et al., 2017; Huang et al., 2017).

The basement of the Central Andes in the study area is made of the Arequipa and the Paracas crustal domains (Ramos, 2008). The Proterozoic Arequipa domain (southern part of the study area) is characterized by gneisses with some Cretaceous and Paleogene granitoid intrusions. The Paleozoic Paracas domain is composed of a variety of gneisses and amphibolites and is thinner with a more sialic comparison than the Arequipa basement (Yuan et al., 2002; Mamani et al., 2008). The boundary between the two domains is delineated by different isotopic compositions of Pb (Mamani et al., 2010). This part of Central Andes consists of epicontinental Jurassic and Cretaceous strata, terrestrial detrital (sandstone, mudstone, and shale) and primary pyroclastic rocks (tuff and lapilli tuffs), Cenozoic deposits including coherent volcanic rocks in various formal stratigraphic units (ignimbrite, tuff, andesite and dacite lavas and conglomerates), and Upper Cretaceous–Neogene intrusive rocks (granitoids; Mégard, 1987; Sébrier and Soler, 1991; Swanson et al., 2004). The high-relief erosional surfaces reveal significant volumes of dacitic ignimbrites (Thouret et al., 2016; de Silva and Kay, 2018) and the common presence of andesitic lava flows spatially associated with dacitic dome and composite volcanoes (Thorpe and Francis, 1979; Klerkx et al., 1979; Trumbull et al., 1999; Kay et al., 2005).

The Andahua Group has been active from the Pleistocene until historical time. Three volcanic intervals have been distinguished (Figs. 1C and 2): the oldest one named Andagua – 0.5 ±0.07 Ma (Pleistocene – generation I), with an eruption of Calera at 0.23 ±0.02 Ma (K/Ar, Kaneoka and Guevara, 1984), an intermediate interval known as Antaymarca at 60 ka (Pleistocene–Holocene – generation II) and the youngest one at 1451 to 1523 A.D. (Cabrera and Thouret, 2000) knowing as Chilcayoc (Holocene to historical times - generation III).

GEOPARK COLCA AND VOLCANOES OF ANDAGUA

The study area is in the Geopark Colca y Volcanoes de Andagua; Fig. 1C). This geopark belongs to the UNESCO Global Geopark network, established to exhibit and protect the various volcanic landforms (Gałaś and Gałaś, 2017). Geotourism in the geopark is organized according to rules ensuring preservation, exhibition and explanation of unique rock outcrops, landscape diversity and geological processes. Economic activities are also directed towards sustainable development.

The area of geopark can be divided into three main parts: the Colca Valley, Colca Canyon and Valley of the Volcanoes. 119 geosites are documented (Zavala and Churata, 2016), with a clear record of structural and sedimentary environments, tectonic deformation, evolution of the area through time, transformation of the surface and deeper in the crust, hot springs, geysers, conditions of soil development, the fluvio-lacustrine network, and various topographic landforms (Gałaś et al., 2018). The youngest volcanic forms of the Andahua Group, which have the highest scientific and aesthetic value, are concentrated in the Valley of the Volcanoes (cluster A). The geopark also includes the youngest, and most recently active in Peru, Sabancaya composite volcano. The possibility of close examination of small volcanoes (scoria cones) is a unique attraction, which is enhanced for field-active visitors.

METHODOLOGY

GEOMORPHOLOGY

The geomorphological analyses performed were based on field studies and 3D models of the volcanic structures created with the SfM (Structure-from-Motion) method: analysis of images taken with a hand-held camera by the authors in 2017. 3D models of the volcanic forms were constructed using the Structure-from-Motion software Agisoft Metascan (https://www.agisoft.com/pdf/metashape-pro_1_5_en.pdf). SfM is the name of the group of algorithms that allows for conversion of 2D images into 3D models (Mali and Kuiry, 2018; Park et al., 2019). SfM algorithms recognise high-contrast features of the objects photographed objects, following their movement through a series of images; this produces a sparse point cloud based on the placements of features (Rayan, 2015). The object surveyed should feature highly contrasted elements that project onto at least a few pictures. JPG and other standard photo files contain embedded metadata making it possible to calculate and implement camera calibration files within the software. Although SfM algorithms allow the construction of 3D models with strong geometrical features, the resulting scales are inaccurate (Lewińska et al., 2021). To create a model with the correct scale, the dimensions or coordinates of certain elements (e.g., GCPs – ground control points) of the object must be provided. In the case of the Valley of the Volcanoes, GCPs were designed as black and white chessboards of exactly 20 20 cm (each black or white square was 1010 cm; Strach et al., 2017). Their coordinates were measured using GNSS dual-frequency units. One was used as a base station (the Arequipa permanent base was used for establishing precise location) and another one as a rover unit (Maciuk, 2016; Maciuk and Szombara, 2018). The GCPs had an average accuracy for XYZ of 4.4 cm.

The SfM survey was conducted in July 2017 and covered a broad area of the Valley of the Volcanoes including the outer slopes of the Chilcayoc, Chilcayoc Grande and Jechapita volcanoes (Fig. 2). These models covered two-thirds of the cones. In addition, a 3D model of the crater and cone of the Chilcayoc Chico and Niñamama volcanoes (Fig. 2) was produced. For the Puca Mauras volcano (Fig. 2), a model of the crater and the cone was created. Additionally, a model of the south and east lava flow that originates from the Puca Mauras volcano was created. For the smaller cones, the accuracy is between 2 and 5 m while for the craters it is 0.5–2 m (XYZ error). For Puca Mauras the cones model had an average XYZ accuracy of ~7 m, and the error for the lava flow models varied from 2 to 15 m. The models were used for better representation of the area, for cross-sections and for validating other spatial data including volume calculations, heights, and slope measurements.

For the volume calculations, SfM models were used along with satellite-based Digital Elevation Models (DEMs) from Shuttle Radar Topography Mission SRTM-X (1") with a resolution of 30 m (Kavanagh et al., 2017). SRT missions give (a) 16 m absolute vertical height accuracy, (b) 10 m relative vertical height accuracy and (c) 20 m absolute horizontal accuracy (Wessling, 1999; González et al., 2011; Fornaciai et al., 2012). Additionally, the ALOS DEM obtained from the Alaska Satellite Facility (ASF) Distributed Active Archive Center (DAAC), was also used. This DEM has a cell size of 12.5 12.5 m (Niipele and Chen, 2019). The height accuracy has been estimated at 5 m (Tadono et al., 2014). Results of all calculations were cross-validated by each DEM and where possible, by the Structure-from-Motion models. A validation process checked whether the numerical results are similar within their respective accuracies.

The DEMs were primarily used for calculating the total volume of each volcanic structure. All calculations were done with QGIS software (https://qgis.org/pl/site/). Since there is no information on how the land looked before each eruption or on the relative ratios between various eruptive products, the calculated volumes are only considered as rough estimates of the bulk volumes. While we have not performed detailed textural analysis on the vesicularity of the pyroclastic and coherent eruptive products, nor determined the possible effects of the surface roughness of lava flows, the volume values provided here, being at least 20% higher than the dense rock equivalent values, are based on analogous volcanic fields elsewhere (Kereszturi et al., 2013). We use two surfaces: the top (the current morphology of the landforms) and the bottom (base surface on what the volcanoes erupted) of the volcanoes. The bottom surface cannot be established directly as it is covered by the lava. Thus, a theoretical surface was created for the volcanoes and lava flows by picking at least 20 reference points on the area close to the cone. Based on the measured elevation and their geographic positions a theoretical bottom reference surface was interpolated and used for further volume calculations of volcanic landforms.

CHRONOLOGICAL CORRELATION

To establish the chronology and relative ages of volcanic activity of the Andahua Group we used published data (Kaneoka and Guevara, 1984; Cabrera and Thouret, 2000; Delacour et al., 2007), geological information that we obtained during field trips (seasons 2003–2017) and remote sensing information utilizing photography, ASTER DEM, and Landsat Satellite images (e.g., Google EarthTM).

A Normalised Difference Vegetation Index (NDVI) estimated the boundaries between volcanic products of different generations. The NDVI enables comparison of seasonal and inter-annual changes in biomass growth and activity (Huete, 1988) using the ratio of the near infrared and red channels (Jensen, 1986). We used it to show the development of soils and vegetation, which reflects the time that has passed since the eruption.

PETROLOGICAL ANALYSES

The petrogenetic models that are given in this paper are based on the chemical analyses of samples collected by the first author (Gałaś, 2014) and supplemented by new samples (collected in 2017) and data published by Delacour et al. (2007, e.g., sample vol6) for rocks located outside of the Valley of the Volcanoes. A total of 130 samples gathered from seven regions, in which the Andahua Group rocks occur, were studied. 50 thin sections for transmitted light microscopy were prepared and analysed. 45 samples were further analysed by ICP-MS and ICP-OES at ACTLABS Activation Laboratories Ltd. (Canada). Major oxides were subsequently normalised to 100%. Trace elements were determined with the following detection limits (ppm): Cr, Ni = 20; Zr = 4; Rb = 2; La, Th = 0.1. Selected samples (14) were analysed by means of *Quanta FEG* and *NOVA NANO SEM 200* electron probe micro-analysers. These comprised initial research into the olivine, amphibole, pyroxene, plagioclase and garnet crystals. Sr-, Nd-isotope TIMS analyses of 9 samples from lavas and Pb-isotope TIMS analyses of 2 samples from lavas were performed using the triton multi-collector mass spectrometer in the static mode. Rb and Sr were

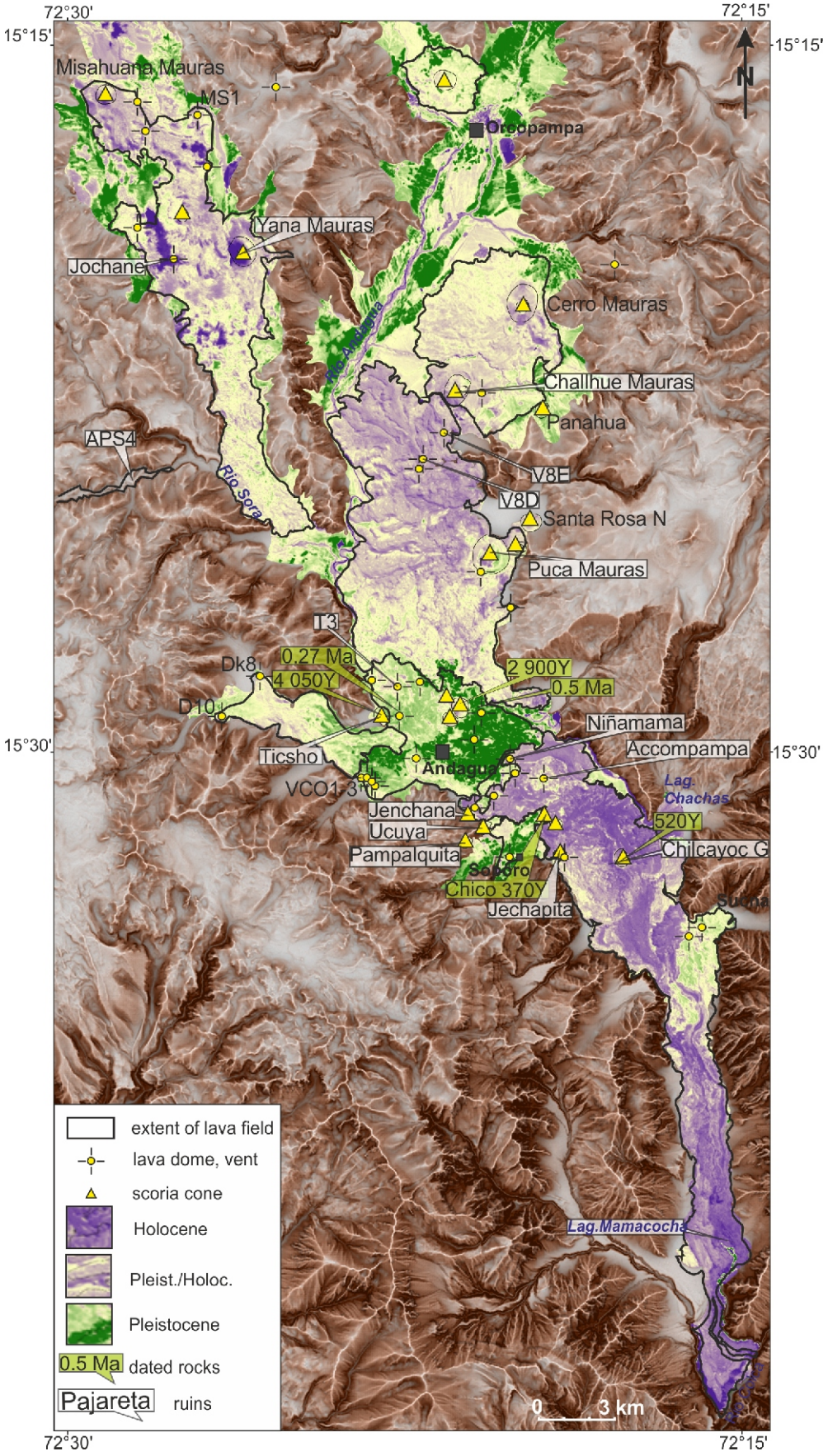

Fig. 2. Age distribution of volcanic products of cluster A (Valley of the Volcanoes; extent of Andahua Group lavas by Gałaś, 2011) interpreted from the state of vegetation by means of a normalized vegetation index NDVI (Normalised Difference Vegetation Index)

Calculated from data from the Landsat 8

Table 1

Quantitative characteristics of Andahua Group volcanoes

Regions	Lava fields	Lava domes and vents	Scoria cones	Composite volcanoes	Volume [km^3]	Age
A. Valley of the Volcanoes	12	41	23	1	19.3	0.5 Ma–recent
B. Antapuna	4	6	3	1	6.4	0.5 Ma–recent
C. Rio Molloco Valley	3	10	1	0	1.7	60 ka
D. Lagoon Parihuana	0	0	6	0	0.07	60 ka
E. Rio Colca Valley	2	11	0	0	0.8	172–0.23 ka
F. Pampa Jarán	5	14	10	1	7.7	0.5 Ma–60 ka
G. Huambo-Cabanaconde	3	21	0	0	5.9	0.5 Ma–2650 BP
Total	**29**	**103**	**43**	**3**	**41.87**	

The ages are based on individual dating (Kaneoka and Guevara, 1984; Eash and Sandor, 1995; Cabrera and Thouret, 2000) correlated with fieldwork data (Gałaś, 2011, modified)

separated by ion-exchange extraction chromatography. Sm and Nd were separated by extraction chromatography on HDEHP-covered teflon powder. Pb was separated using the ion-exchange technique with Bio-Rad 1 8. During the analyses the $^{87}Sr/^{86}Sr$ ratio of the NBS 987 standard was 0.710248 ±0.000008 and the $^{143}Nd/^{144}Nd$ JNd-1 standard ratio was 0.5121049 ±0.000018. External reproducibility of lead isotope ratios – $^{206}Pb/^{204}Pb$ = 0.1%, $^{207}Pb/^{204}Pb$ = 0.1%, $^{208}Pb/^{204}Pb$ = 0.2% – at the 2 level has been demonstrated through multiple analyses of standard BCR-1.

Three samples from Mamani et al. (2008), namely BAS21 (Charcani gneisses – Arequipa domain), OCO0708 (amphibolite – Paracas domain) and OCO0703 (granite – Paracas domain; Appendix 1), were also included in model calculations.

The petrological model calculations were made using the *Petrograph* program (https://petrograph.software.informer.com/2.0/; Petrelli et al., 2005).

RESULTS

MORPHOLOGY OF VOLCANIC LANDFORMS AND AGE CORRELATION

The Andahua Group's seven clusters of volcanic eruption centres is located on both sides of the Colca Canyon (Fig. 1C). Each cluster contains several lava fields composed of successive lava flows, small lava domes, lava vents and pyroclastic cones. The total number of volcanic centres identified in this study is 149 (Table 1 and Appendix 2).

As many as 29 lava vents (all Pleistocene) were not assigned to the types defined due to erosion and uncertainties regarding their original shape. Several may be cryptodomes or tumuli (Mattsson and Hoskuldsson, 2005; Németh et al., 2008), previously described as vents (Gałaś, 2011).

LAVA DOMES

These volcanoes are aligned along feeding fissures that can be recognized in the field and from satellite imagery by the presence of distinct fracture zones, the radial dip directions of lava spatter piles and coherent lava units. Morphological analysis indicates that the domes have structural differences varying from platy and spiny to axisymmetrical landforms (Fig. 3). They can be the source of a single flow (type 1A), several lava flows that poured out in different directions or multiple injection–controlled, Christmas tree-types of domes (type 1B), and lava domes that were active more than once with visible stages of growth (type 1C). Type 1A: the flow of relatively viscous lava resulted in the formation of a dome ~100 metres high. The lava then flowed in one direction, following the slope, or to form a wide fan. A breached crater with sharp lava walls on its inner parts is often seen. On the surface of the dome, the lava flows have agglutinated characteristics. Type 1B is characterized by more than one lava flow that originated from a single dome. Flow structures indicate that the lava did not tear the dome apart but continued to flow in different directions from the dome. The 1C-type dome has visible structures inside the crater. These indicate the inflow of the next batch of lava and the formation of a smaller structure inside the older one. The structure of the lava flow also indicates more than one outflow event from the dome.

Some landforms that are incised by erosion show an interior that is built of massive lava. These are distinct hills, and the location of the lava flows indicates that they were their source. The Andahua Group domes, with limited erosion, are 20–150 m in height. The slope angles of the lava domes measured range between 28 and 39°.

As an example, the total edifice bulk volume of a lava dome (type 1A) such as the Chipchane dome (Fig. 4), is 0.3 km^3. The lava field created from the two V8C-D lava domes (type 1B) has a volume of ~1.5 km^3.

A few volcanic forms of different shape and size have also been observed. A unique feature for the Andahua Group is seen in the lava dome called Cerro Coropuna in cluster C (Fig. 1C). It breaks through the lava cover in a small hanging valley above the Rio Molloco Valley. It reaches a relative height of 250 m, and its slope angle ranges between 39 and 43°. It is composed of lava blocks, and closely resembles Pelean-type lava domes (Fink and Griffiths, 1998).

Of the lava domes, 40 are type 1A domes (Fig. 5), while 26 were classified as type 1B domes and 7 as type 1C.

SCORIA CONES

Other volcanic landform types are small to medium sized scoria cones, which can be divided into the following groups (Fig. 6, Table 1 and Appendix 2): simple, symmetrical volcanoes (type 2A), cones breached by lava flow (type 2B), and

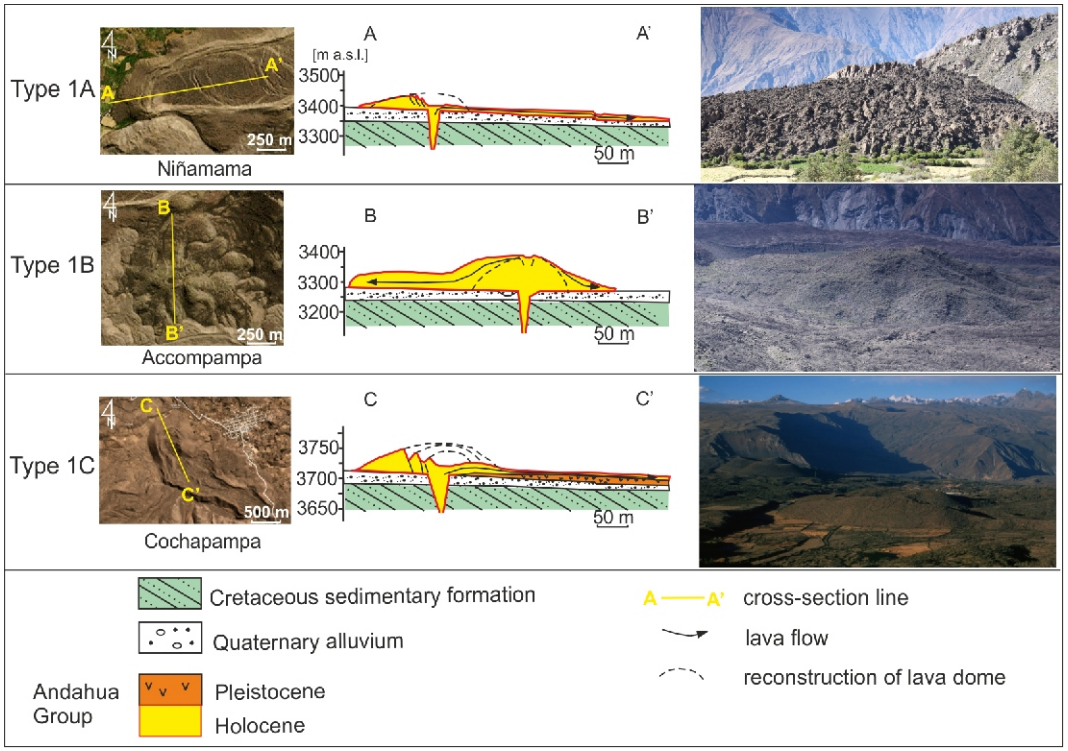

Fig. 3. View and simplified geological cross-section of Andahua Group different lava dome types

For location of selected lava domes see Figure 4

complex shape - multi-active cones (type 2C). The 2A type is built by alternations of lapilli-to block size pyroclasts and/or lava spatter. The sides of the scoria cones are steep, and they have shallow craters. They are dominated by collars of lava spatter around their craters and are typically dominated by pyroclastic material along their base (Dóniz-Páez et al., 2012). Type 2B originally developed as a cone type 2A, followed by injection of lava into the crater. Lava could flow out if it compromised the stability of the walls and breached the cone. Or when it poured over the rim of the crater, it breached the cone's wall and flowed out. Type 2C is distinguished by structures that indicate a change in the strength of eruption and a change in its character. Crater edges inserted into larger craters, or lava effusions that flowed out of the cone after its partial breach, are observed. The Andahua Group scoria cones have a relative height of 50 to 170 m. The cones were formed by repeated Strombolian-style explosive eruptions. The external slope angle for most of the measured cones (31 from 42) ranges between 28 and 36°. The edifice volume of the scoria cones is usually small, on the order of 0.002–0.1 km^3 with only two exceptions. The largest one, Puca Mauras (Fig. 4), has a volume of 0.15 km^3 and Cerro Mauras 0.13 km^3. In total, 23 cones are type 2A, while only 5 are type 2B cones (Ucuya, Pampalquita, Chilcayoc, Cerro Pucqguada), 3 type 2C (Cerro Mauras, Ticsho, Jenchaña) and a single cone (Chico) shows features of type B and C.

Only five cones could be described as having a compound eruption history: Strombolian type eruption and effusive activity (type 2B).

Twelve other cones of different age were also observed (Smoll et al., 1997; Gałaś, 2011). However, they were observed as parts of previous volcanic structures. Therefore, none of them could be classified according to types A–C.

Next to the cones there are plains of black volcanic ash. Ash from older eruptions is overlain by soil and in places colluvium. The youngest ashes appear at the surface. The thickness of the cover is usually 0.5 m, but it can reach up to 2 m (e.g., near the Gloriahuasi volcano; Fig. 1). In addition to the ash, the cover also contains lapilli and small volcanic bombs.

POLYGENETIC VOLCANOES

Some volcanoes of the Andahua Group are classified as monogenetic based on their edifice/eruptive volume, simplicity of volcanic architecture and the lack of evidence for time hiatuses within their eruptive products (Delacour et al., 2007). However, not all the volcanoes share these monogenetic characteristics. The greater part volume of the products of volcanic activity and the rejuvenation of activity after thousands of years indicates that there are volcanoes with polygenetic features in the Andahua Group. There are several complex volcanoes that cannot be classified as a typical monogenetic volcano, such as Gloriahuasi, Puca Mauras and Ticsho (Figs. 1, 4 and 6, Table 1, Appendix 2).

There are also two volcanoes (Antapuna and Gloriahuasi) built of layers of lava and pyroclastic rocks. Their heights are 190 m for Antapuna and 412 m for Gloriahuasi – 412 m. Located within clusters B and F, respectively (Fig. 1C), they are rather small composite volcanoes.

Puca Mauras in the Valley of the Volcanoes can be considered as the best example of a typical complex volcano with a few eruption phases, a changing eruption style and a larger volume than those of monogenetic (Fig. 4). Lava occupies the entire width (~4–6 km) and length of a 16 km long valley to the north of the village of Andagua. The main eruption centres are

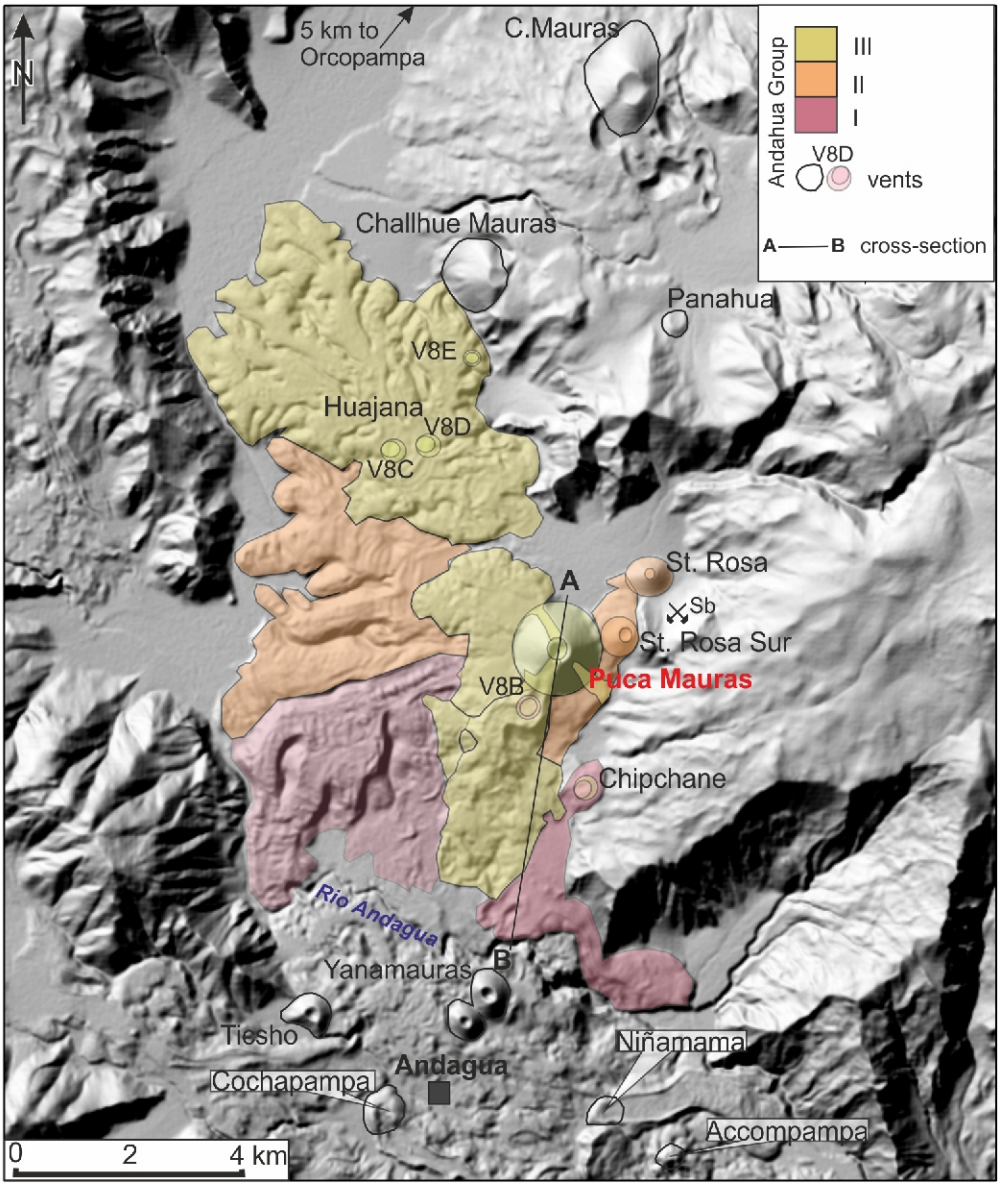

Fig. 4. Map of Puca Mauras complex, active during Late Pleistocene (Generation II)

Lava flows emplaced during I–III eruptive episodes; for location of cross-section A–B see Figure 7

located at the eastern edge of the valley near the inactive Santa Rosa antimony mine (Fig. 4). They can also consist of voluminous and extensive lava flows that were erupted from either one or a group of vents or are derived from breached scoria cones. The lava flows from the V8B lava dome (type 1C), created in separate episodes (Figs. 2 and 4), and running into the Puca Mauras cone, have a bulk volume of >3 km^3. Lava flows and volcanic ash cover an area of ~70 km^2. The lava flows originated from three large (V8B, V8C, V8D) and one small lava domes (V8E). The lava flowed radially to the north, west and south to form a 100–150 m thick cover with numerous lobes (Fig. 7). The longest flow is ~10 km long and 2 km wide (Gałaś, 2008). Three pyroclastic cones, including the largest in the Valley of the Volcanoes – Puca Mauras – formed the youngest eruptions. The Puca Mauras cone has a relative height of 350 m, a crater with a diameter of 300 and a depth of 80 m. The crater's rim has a 50 m-deep breach through which lava exited. The lower part of the cone is made of strongly weathered volcanic rocks, as clasts 1 mm across or smaller. The younger, upper part of the cone is made of fresh lapilli, blocks and bombs. The other two monogenetic cones, Santa Rosa (100 m high) and Santa Rosa Sur (50 m), form the perimeter of the Valley of the Volcanoes' ditch. Compared to the other Andahua Group volcanoes, the presence of the most complex lava domes and the largest scoria cones suggest that these eruptions were the most voluminous and potentially the longest-lived in the area.

PETROGRAPHY AND GEOCHEMISTRY

The lavas of the Andahua Group have hypocrystalline-porphyritic texture. The phenocrysts and microphenocrysts are mainly represented by plagioclase although olivine, clinopyroxene and amphibole are also present. The plagioclase reaches sizes up to 5 mm, olivine up to 2 mm, clinopyroxene up to 1.5 mm and amphibole to 4 mm. The groundmass is intergranular, pilotaxic, felty or hyalopilitic with microlites composed of

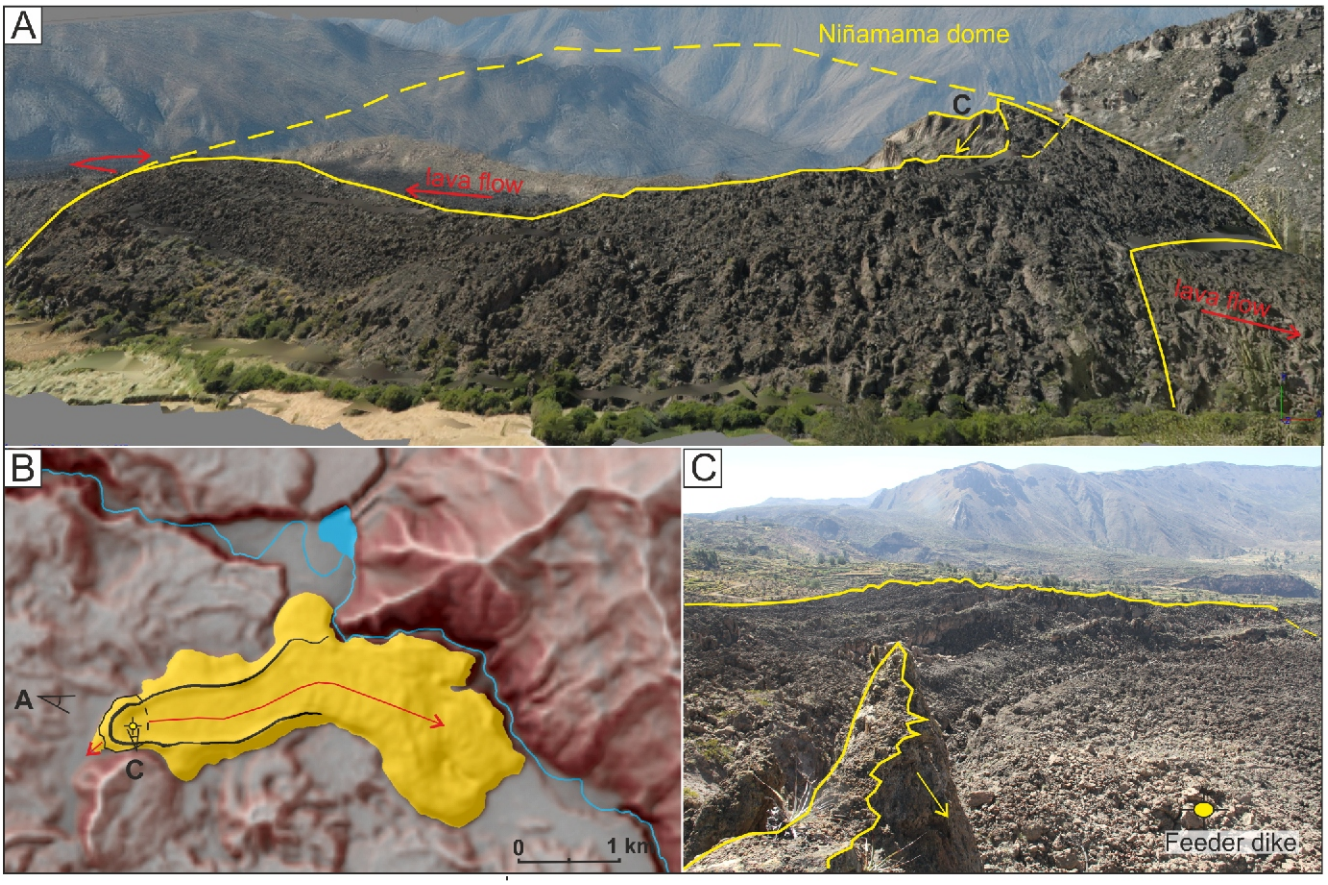

Fig. 5. Niñamama dome

A – mesh model with photo-realistic texture; height from the base to the preserved rim 60 m; yellow, dotted line means reconstruction; view from the north; **B** – lava flow poured from Niñamama dome highlighted on a Red Relief Image Map; the place where photo C was taken is marked; **C** – view from the western rim of the collapsed part of the dome with a feeder dike (analogue photo)

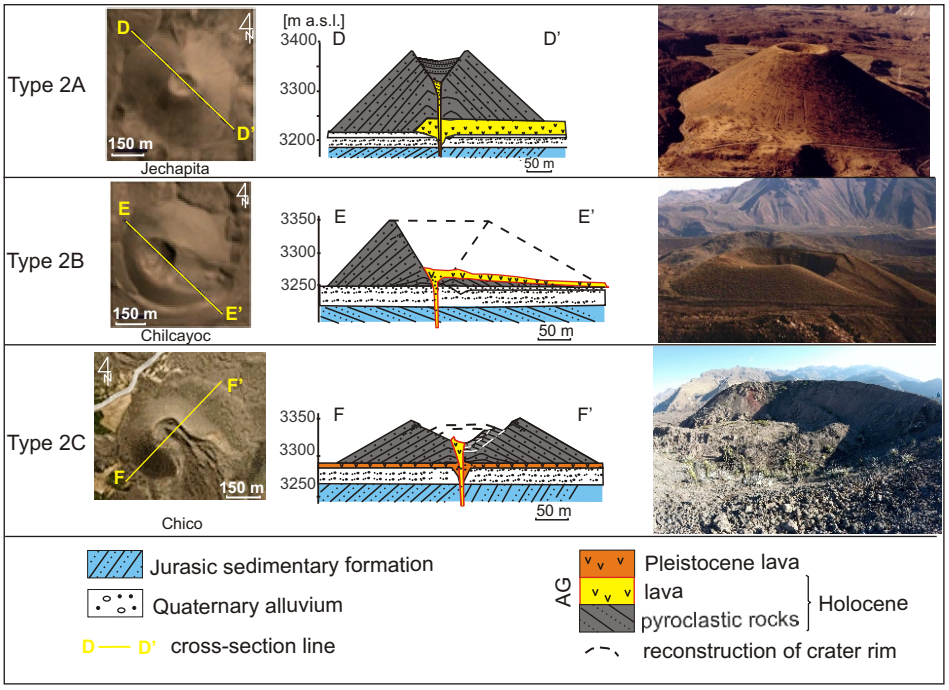

Fig. 6. View and simplified geological cross-section of Andahua Group scoria cones types

For location of selected scoria cones see Figure 2

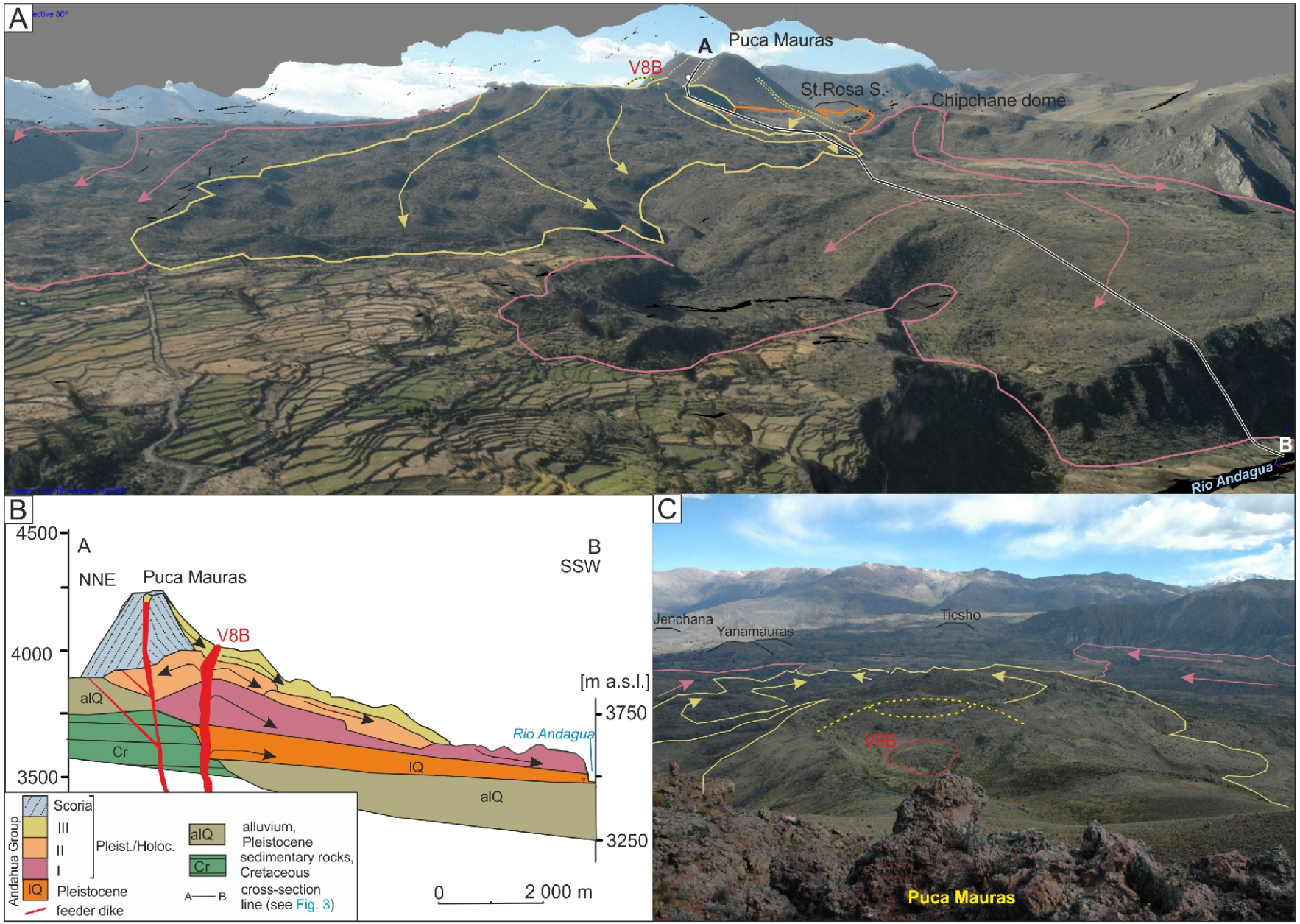

Fig. 7. Puca Mauras lava field with the interpretation of the range and chronology of lava flow

A – mesh model with photo-realistic texture, view from the south, from the Jemellos volcano; **B** – geological cross-section, twice vertical exaggeration, I–III Andahua Group episodes of activity; **C** – view from the southern rim of the Puca Mauras crater to south (analogue photo), yellow, dotted line means reconstruction of lava dome V8B, and red, dotted line means relict of V8B lava dome

plagioclase, pyroxene, oxides and locally olivine. In contrast, the dominant phenocrysts within the lavas from the Puca Mauras lava field are plagioclase and minor amphibole although magnetite is also present. Most of the amphibole crystals are replaced by secondary oxides. They contain magnetite as phenocrysts, microphenocrysts and microlites.

In petrological terms, the products of the Andahua Group volcanoes are basaltic andesites, andesites and dacites (Fig. 8). Using the TAS diagram (Le Maitre et al., 1989) these are respectively classified as basaltic andesites, basaltic trachyandesites, trachyandesites (latites) and trachydacites (Gałaś, 2014).

In the basaltic trachyandesites, amphibole and olivine comprise the dominate phenocrysts and microphenocrysts but are also accompanied by plagioclase. The euhedral olivine crystals exhibit numerous cracks and fragmented edges (Fig. 9A) and are covered by rims of iddingsite and goethite. The composition of the olivine ranges from Fo_{74} (core) to Fo_{62} (rim). The composition of plagioclase phenocrysts ranges from An_{44} to An_{71} (Delacour et al., 2007) and from An_{48} to An_{67} in the microcrystalline groundmass (Gałaś, 2014). Occurrences of pyroxene in the form of diopside, augite ($Wo_{38}En_{47}Fs_{13}$) and enstatite ($Wo_4En_{73}Fs_{23}$) have also been recorded.

In the trachyandesites, plagioclase dominates, with minor amphibole and pyroxene. The plagioclase shows signs of melting and contains fluid inclusions, rarely showing marked zoning (Fig. 9B). In addition, the amphibole shows signs of changes and corrosion with embayments that are filled with a finely crystalline groundmass (Fig. 9C). The grains of clinopyroxene are hipautomorphic (small pyroxenes are also present in the groundmass) with small compositional changes: $Wo_{36-43}En_{43-52}Fs_{10-15}$ (Gałaś, 2014).

The trachydacites contain plagioclase and amphibole. The plagioclase has a chemical composition in the oligoclase-andesine field and contains more Ca than the plagioclase of the groundmass.

Several samples contain various types of upper crustal xenoliths. Thes represent rock fragments of granodiorite with diverse crystal sizes from the Arequipa Massif (Proterozoic) (sample from Gloriahuasi volcano) and quartzite (Cochapampa) as well as broken metamorphic quartz crystals (Marhuas volcano) derived from Mesozoic quartzites (Yura or Murco formations). In lavas from the Huajana lava dome (V8C, Fig. 3), andraditic garnet glomerocrysts (Puca Mauras lava field) are common. They show a complex zoning pattern with mottled cores, oscillatory mantles (enriched in Ca and Al) and unzoned rims. They host a few inclusions of anhydrite, halite, S- and Cl-bearing silicate glass, quartzite, anorthite, wollastonite and magnetite (Gałaś et al., 2021).

The SiO_2 content of the Andahua Group lavas ranges from 52 to 68 vol.% (Fig. 8). The rocks lie within the high-K calc-alkaline series with a prevalence of sodium over potassium. The Andahua Group lavas are enriched in light REE. More details on the samples and petrology of Andahua Group are available in Gałaś (2014).

PETROGENETIC MODELLING

The models presented here are based on a representative set of samples (Appendix 2) taken from the Andahua Group volcanic clusters (Fig. 1C). The models consider the Charcani Gneisses from the Arequipa domain and granitoids from the Paracas domain as possible sources of contamination. Mesozoic sedimentary rocks are also treated as contaminants (although not strictly included in the models). They also consider the wide dispersion of Andahua Group volcanic activity in both time (generations I–III) and space (clusters A–G).

FRACTIONAL CRYSTALLIZATION (FC)

Fractional crystallization equations (Rayleigh equation) were applied to the modelling of trace elements. Fractional crystallization of plagioclase, amphibole and Ti-magnetite was inferred in the primitive, basic magma. The role of fractional crystallization suggests: the presence of zoned plagioclase phenocrysts and correlation between incompatible elements. A relatively narrow range of $^{87}Sr/^{86}Sr$ values (Appendix 3) indicates initially one source of primitive magma. The most primitive lava in this part of the CVZ (sample vol6, Delacour et al., 2007) fits perfectly between the projections of the components of the rock samples from the Andahua Group lavas. The “vol6” sample, with 7.3 vol.% content of MgO (Appendix 1), was used to model the initial magma in the deep crustal reservoir. Similar assumptions have been made in other analyses, regarding the parental magmas of the Central Andes reveal basaltic rocks (James et al., 1976; Klerkx et al., 1979; Wilson, 1989).

The partition coefficients used for the basalts and basaltic andesites are shown in Table 2. Using the mass-balance algorithm of Störmer and Nicholls (1978), the ratio of the minerals crystallising from the magma was calculated to be 50.22 vol.% Pl + 46.97 vol.% Amp + 2.81 vol.% Ti-Mag. The values of r2 = 0.8814 show acceptable correlation between the model and data (Janoušek et al., 2015). The result of these calculations is that: (a) olivine and pyroxene do not play a significant role in the fractional crystallisation process; and (b) fractional crystallization of plagioclase, clinopyroxene and amphibole from basaltic andesites to trachyandesites is very likely.

The first section of the FC-trend (Fig. 10A) does not coincide with the projection of samples. This is due to the low-Zr AG lavas that are also relatively poor in Cr (Appendix 2). The Cr vs. Zr curves only partly correlate with the FC-modelled trend, i.e., that regarding to the most basic and Zr-poor rocks of the AG (Fig.10A). Since, in olivine and clinopyroxene, Zr is an incompatible element and Cr is a compatible element, this supports the thesis that fractionation of these mineral phases is not of great importance. Considering the Sr vs. Rb and Zr vs. Rb trends, their FC model curves provides no fit whatsoever (Fig. 11A, B).

The fractional crystallization of potentially important minerals (plagioclase and amphibole) has a supporting or minimal role in differentiation of magmas that is observed in lavas of the Andahua Group. Figures 10 and 11 suggest that fractional crystallization has been recorded in the first generation of lavas from the Pampa Jarn cluster.

ASSIMILATION AND FRACTIONAL CRYSTALLIZATION (AFC)

The distinct positive correlations of $^{87}Sr/^{86}Sr$ ratios to SiO_2 content and negative $^{143}Nd/^{144}Nd$ ratios to SiO_2 content in lavas of the Andahua Group (Gałaś, 2014) suggest the important role of crustal contamination in magma evolution. One of the indications of contamination by sedimentary rocks, xenocrysts, which contain andraditic garnet, has been discovered in the Andahua Group lava agglomerates. These are only found in one place and were determined to be a product of interaction of the magma with evaporites (Gałaś et al., 2021).

The calculation of the AFC model was based on equations from De Paolo (1981). The same sample vol6 magma as previously considered in the FC model was used for the parent material in this model. The AFC equation was derived considering that both parameters, *r* (the ratio of the rate of assimilation to the rate of fractional crystallization) and *D* (the bulk distribution coefficient), are constant (Wilson, 1989).

James (1982) prepared the first AFC models for the northern part of the CVZ. As a contaminant, he identified the Char-

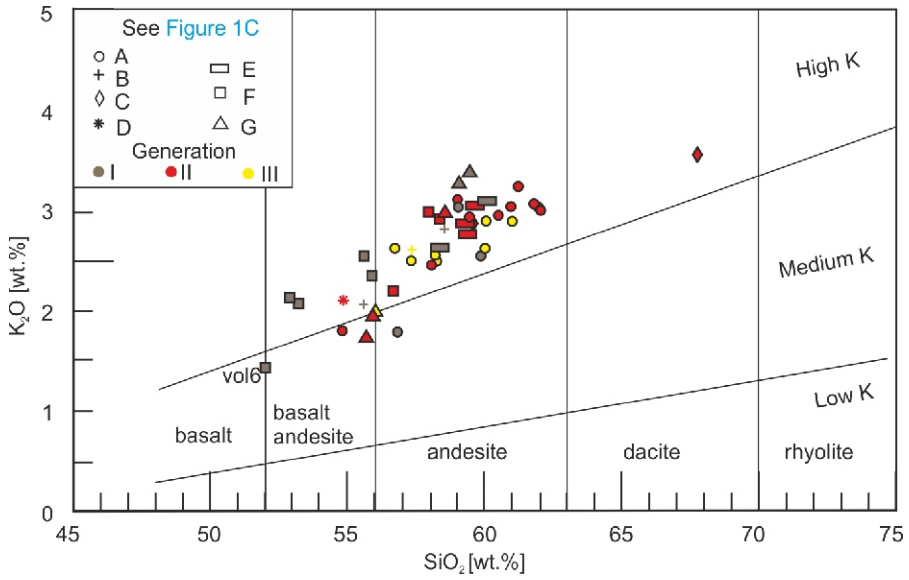

Fig. 8. Plot of K_2O *versus* SiO_2 contents (wt.%) for Andahua Group

Calcalkaline series classification is from Le Maitre (1989); oxide contents are recalculated to 100% on a volatile – free basis; generation: I – Pleistocene, II – Pleistocene–Holocene, III – Holocene

cani Gneisses belonging to the Arequipa Massif. A similar AFC model (the Charcani Gneiss being considered as a contaminant) was also proposed (Samaniego et al., 2016) for the Sabancaya stratovolcano, which is located south of Colca Canyon (Fig.1C). Subsequent authors (Delacour et al., 2007; Sørensen and Holm, 2008) did the same to describe the AFC processes for the Andahua Group. We considered here the possibility of another contaminant, i.e., the granites and amphibolites of the Paracas Massif that occur in the basement of the central and northern part of the study area (Mamani et al., 2008). The AFC1 submodel assumes the Charcani Gneisses as a contaminant, while the AFC2 sub-model assumes granitoids of the Paracas Massif as a contaminant.

The Paracas Massif is characterized by a thinner underlying crust that is described as less mafic than that located to the south of the Arequipa Massif (Mamani et al., 2008). Distinct differences between $^{206}Pb/^{204}Pb$ and $^{87}Sr/^{86}Sr$ ratios (Delacour et al., 2007 and Appendix 2) for the eruption products from the Huambo region (Fig. 12; cluster G) and those from the Valley of the Volcanoes (A) or Antapuna (cluster B) suggest the presence of a suture between these two massifs along the Colca Canyon line (Mamani et al., 2010). The Paracas domain rocks, considered here as contaminants, are significantly different in their content of trace elements to the lavas of the Andahua Group. They contain higher amounts of Zr, Nb and Th (Appendix 1).

Interestingly, the Puca Mauras volcano (cluster A Valle of the Volcanoes) and its products show a ratio of $^{206}Pb/^{204}Pb$ isotopes (Fig. 12; Delacour et al. 2007) typical of the transition zone between the Arequipa and Paracas domains. Additionally, south of Puca Mauras, although a continuation of the transition zone could be expected, the lavas of the Andahua Group up to the south side of the Colca Canyon show the same chemical features as those of the Paracas domain (Fig. 12). Probably the northern boundaries of the transition zone (Mamani et al., 2010) are defined by the lava flows of the Sora Valley (APS4) and the Puca Mauras (Fig. 2), which have values typical of the Paracas domain.

These are indications that the Paracas Massif has a dominant role in the contamination of the magma feeding the volcanoes of the Andahua Group. The southern boundary of the Paracas Massif possibly lies south of the Colca Canyon.

A low ratio of $^{87}Sr/^{86}Sr$ (Appendix 3) likely implies a low amount of contamination as the Charcani Gneisses and Paracas granitoids have a higher Sr isotopic ratio. The melting of these rocks could have contaminated the magmas that were supplying the volcanoes of the AG, leading to elevated Sr and Pb isotope ratios (Mamani et al., 2010; Gałaś, 2014).

From the relations between Cr, La and Zr, it is possible to draw conclusions regarding the evolution of the assimilation processes (Fig. 10). In the AFC submodels considered here, the ratio (*r*) between the assimilation and fractional crystallization rates has been set at 0.15 (Aitcheson and Forrest, 1994).

Evaluation of the fit of the numerical models on the plot indicates that assimilation and fractional crystallization are most probably both significant to the evolution of the Andahua Group lavas. The course of the curves of both models is relatively close, which is not surprising due to the geochemical similarity

Table 2

Mineral/melt partition coefficients (Anderson and Greenland, 1969; Burke et al., 1982; Bacon and Druitt, 1988; Baker and Wyllie, 1992; Rollinson, 1993; Ewart and Griffin, 1994; Dun and Sen, 1999) used for the FC, AFC1 and AFC2 magma evolution models

	Pl	Amp	Mag
Sr	0.28	0.01	0.11
Zr	0.2	0.5	0.38
Rb	0.056	0.02	–
La	0.075	0.045	0.0029
Cr	0.25	2.5	66
V	0.47	3	4
Th	0.01	0.16	–

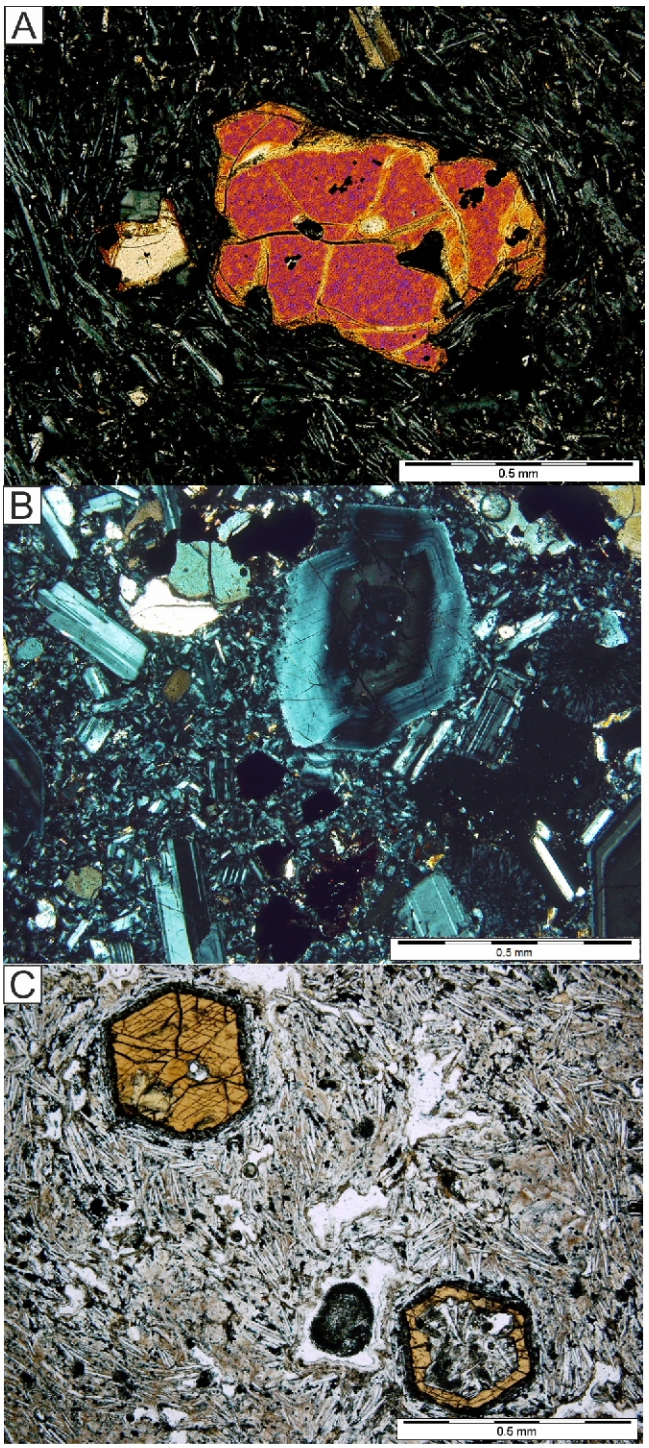

Fig. 9. Photomicrographs of trachyandesite lavas of the Andahua Group

A – olivine in no. H44 (F cluster); **B** – feldspar with marked zoning in no. VO2 (G cluster); **C** – latite from the Valley of the Volcanoes (sample no. DK3), oxyhornblende phenocrysts in microcrystalline groundmass with weakly expressed fluidal texture

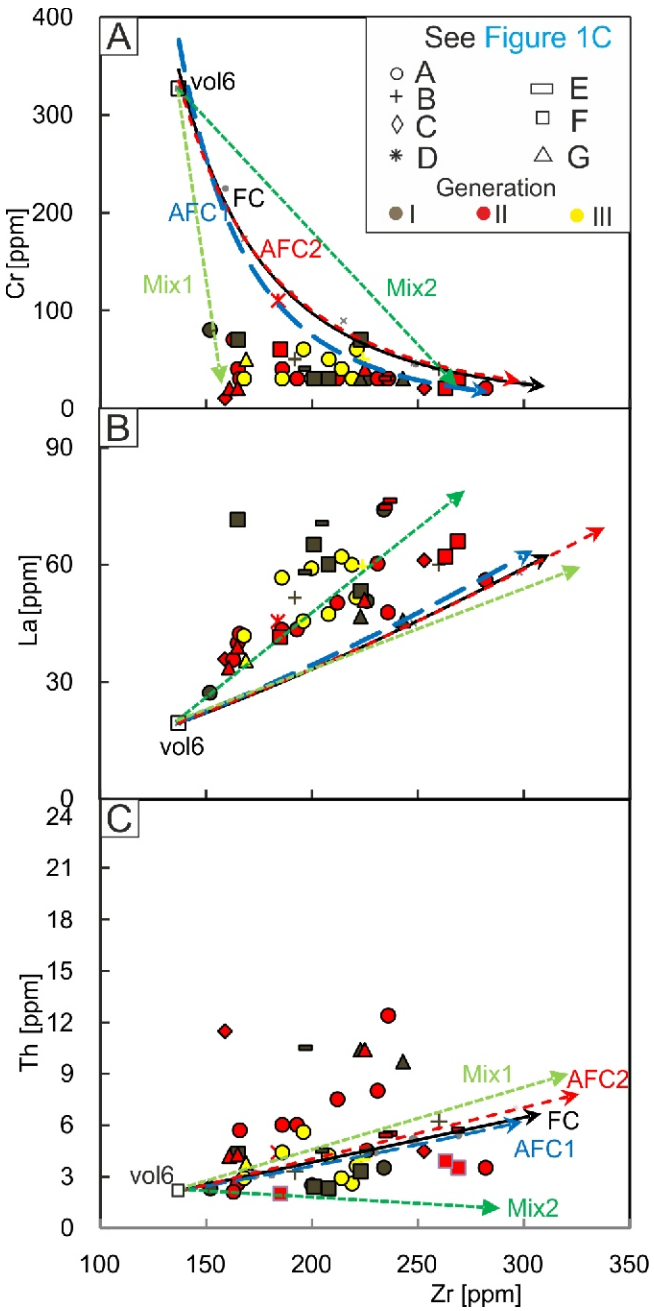

Fig. 10. Variation diagrams for a suite of Andahua Group rocks with the curves of petrogenetic models

FC – fractional crystallization, AFC(1–2) – assimilation and fractional crystallization, Mix1 and Mix2 – mixing; clusters of the Andahua Group rocks (Fig. 1C): A – Valley of the Volcanoes, B – Antapuna, C – Río Molloco, D – Laguna Pariuhuana, E – Río Colca Valley, F – Jaran, G – Huambo (vol6 after Delacour et al., 2007)

of these two massifs. In both models the AFC1 and AFC2 fit relatively well into the Andahua Group product point cloud (Figs. 10 and 11). The AFC2 submodel is the slightly better fitted (Figs. 10 and 11), in both space (correlates with samples from several of the Andahua Group clusters) and in time (correlates with samples from all Andahua Groupgenerations). This indicates a higher degree of contamination from the Paracas granitoids. A change follows to AFC1 for the youngest eruptions, where they are better fitted to other contaminants such as the Charcani Gneisses.

The Andahua Group magmas possibly formed in several chambers located at various depths and were consequently surrounded by rocks with different compositions. As a result, the magmas in the separate chambers could assimilate various components from the local country rocks and the resulting proportions of molten components could also vary. The lack of

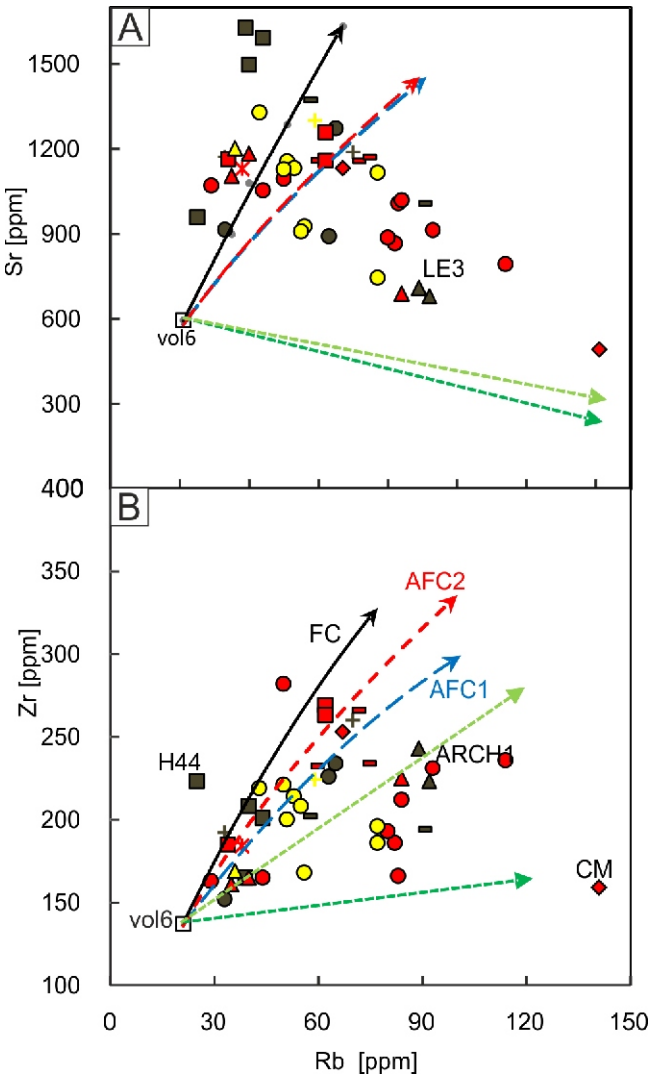

Fig. 11. Variation diagram for a suite of Andahua Group with the curves of the petrogenetic models FC, AFC1 (Charcani Gneisses as a contaminant), AFC2 (granitoids of the Paracas Massif as a contaminant), Mix1–2

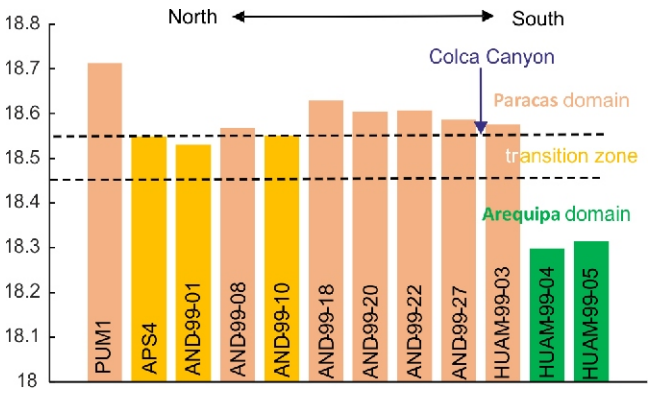

Fig. 12. Variation in $^{206}Pb/^{204}Pb$ of AG with influence of crustal domains

Arequipa – green ($16.083<^{206}Pb/^{204}Pb<18.453$), Paracas – pink ($^{206}Pb/^{204}Pb>18.551$) and transition zone – yellow ($18.453<^{206}Pb/^{204}Pb<18.551$) Mamani et al. (2010), samples AND-…and HUAM-… after Delacour et al. (2007)

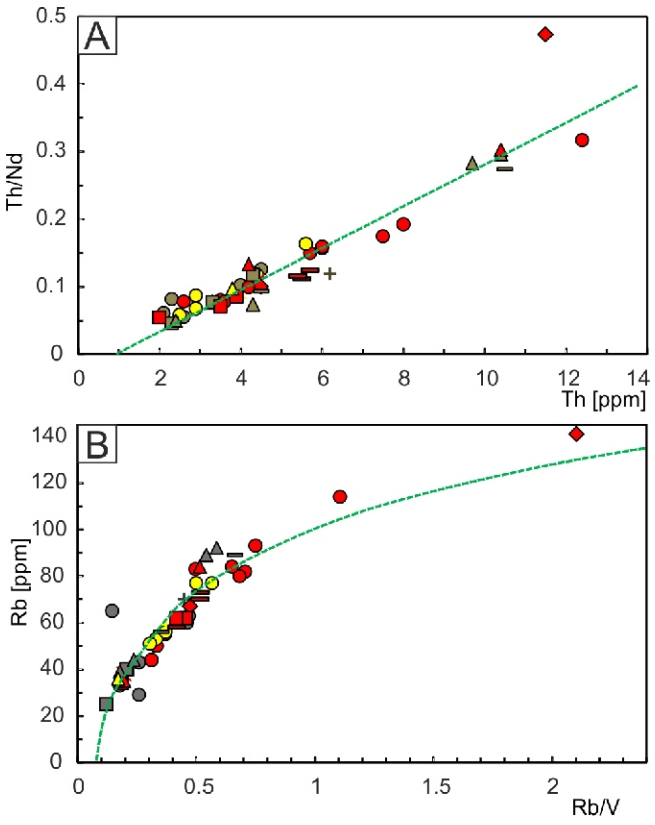

Fig. 13. Plot of highly incompatible trace element

A – Th/Nd vs. Nd with linear correlation; **B** – Rb vs. Rb/V for the Andahua Group lavas with mixing hyperbola

clear differences between AFC1 and AFC2 is due to the presence of a wide transition zone (between the Arequipa and Paracas domains), where both domains affect (Fig. 12), albeit to a different degree, magma differentiation.

MAGMA MIXING

The linear correlation of the Andahua Group lavas on Figure 13A and curves on Figure 13B show the theoretical melt composition produced by mixing. When data lie on straight lines (Fig. 13A) they represent partial melting or mixing, although minor fractionation can contribute to the scatter. Relationships on Figure 13B define curve arrays, which can be interpreted as mixing hyperbolas.

We accepted that a deep located reservoir was filled with mantle magma of hypothetical vol6 composition, i.e., the composition already applied in previous (FC and AFC, Appendix 1) considerations. We tested the case of basaltic magma mixing in an open magma chamber with dacitic magma. The possibility of mixing with dacitic magma, which had features like Charcani Gneisses (Mix1) and Paracas granitoids (Mix2), was tested. As a result, new hybrid magmas could form due to the mixing of mantle magma with the more silicic magma. The trends of both models (Mix1 and Mix2) do not fit well, although the Mix1 model correlates to some degree with the samples with a low Zr content, and the Mix2 model with the samples with a high Zr content.

Despite many attempts, it was not possible to work out a mixing model that would better fit the data. In the Andahua Group magmas, probably the mixing of magma takes place at a very small scale, and other processes may exert more influence on the lava composition.

VOLCANIC EVOLUTION

In this section we attempt a temporal ordering of events, volcanic landform generation and associated magma compositions. The volcanic centres of the Andahua Group formed in three evolutionary steps. In chronological order, these generations occurred in (I) Pleistocene, (II) Pleistocene/Holocene and (III) Late Holocene time.

GENERATION I (0.5–0.126 MA)

The first generation of the Andahua Group activity formed in the central and northern part of the Valley of the Volcanoes (cluster A, see Fig. 1), Antapuna (B), Rio Colca Valley (E), Pampa Jarán (F) and in Huambo-Cabanaconde (G). K-Ar whole-rock analysis of the old volcanic products (Kaneoka and Guevara, 1984) showed that the age of Andahua Group lavas can be estimated as 0.5 Ma for the central part of the Valley of the Volcanoes (Appendix 2). Lava from the opposite end of the field, around the Ticsho volcano (Fig. 4), was dated by the K-Ar whole-rock method and its age estimated at 0.27 Ma (Kaneoka and Guevara, 1984). These dates should be interpreted as separate periods of activity, as the lava in the Colca Valley was dated at 0.4 and 0.23 Ma (Kaneoka and Guevara, 1984). The lava surfaces are weathered and soil-covered. The old generation (Pleistocene) of lavas in the AG are vegetation-covered and often transformed into agricultural fields (Fig. 2).

Despite significant erosion of volcanic forms of the first generation, 33 lava domes, 29 lava vents (undefined type) and 17 scoria cones were recognized (Table 1). In the central part of the Valley of the Volcanoes lava flow fields are present in the area of Andagua and the village of Misahuanca (Figs. 1C and 2). A lava flow field is also known in the side valley of the Rio Tambo (Appendix 2 – D10, Dk8) and it is inferred to be sourced from monogenetic vents above Soporo (Fig. 2). There are also scoria cones (Pampalquita, Ucuya) that were formed during the same period above Soporo. However, during this time, scoria cones (6) also formed in the Pampa Jarán (cluster F). A much greater intensity of eruptions is confirmed by the presence of two complex volcanic landforms. These are the Gloriahuasi (cluster F) and Antapuna (4890 m a.s.l., cluster B) volcanoes, both built as typical composite volcanoes (Fig. 1C). In the strongly glacially eroded Antapuna massif, parasitic cones are observed on the southeastern flank of the complex Antapuna volcano. It is the largest volcanic form of the AG formed in this period.

The products of this eruptive generation correspond to basaltic trachyandesites – trachyandesites, which are the most basic (52.13–53.51 vol.% of SiO_2) in the whole population of the Andahua Group products (Gałaś, 2014). Delacour et al. (2007) described lavas from Pampa Jarán (cluster F) as olivine-rich basaltic andesites. The mineralogical-geochemical nature of the lava from Pampa Jarán suggests that probably they came from little-differentiated magma, evolved during fractional crystallisation (Fig. 10).

In the rest of the lava from this Andahua Group, the presence of olivine, and the geochemical and isotopic composition, suggest a low degree of crustal contamination during the magmatic evolution of the Andahua Group volcanoes (Appendix 2). The results obtained suggest the influence of contamination from both the Arequipa and Paracas domains (Fig. 14).

GENERATION II (172–10 KA)

This generation represents activity in all the clusters of the Andahua Group with the exception of the Antapuna Massif (B cluster). Published ages (K-Ar analysis by Kaneoka and Guevara, 1984; Eash and Sandor, 1995) indicate possible eruptive activity at 172 ka, 95 ka, 64 ka and 60 ka. The previously mentioned Antaymarca volcano was dated 60 ka. For lavas from Puca Mauras, a relative eruption time of <13,000 years BP was determined (Huang et al., 2017).

In the second generation, 31 lava domes and 13 scoria cones were identified (Table 1). Large eruptions are inferred to have taken place in the Valley of the Volcanoes and Huambo-Cabanaconde (clusters A and G, Fig. 1C). In the Valley of the Volcanoes, north of Andagua, there is a large lava flow field previously described as the Puca Mauras complex (Figs. 2, 4 and 7). The lava flow field covers an area of ~70 km^2 with a maximum thickness up to 400 m. The total volume of the volcanic complex is estimated to be ~5 km^3. Similar, but smaller, volcanic complexes are composed of several lava flows that entered the neighbouring Sora Valley (Fig. 2) and on the southern side of the Colca Canyon in the “cluster G”.

In this generation, unusual for this Group, the classic Peleean lava dome type (Francis and Oppenheimer, 2004) deserves attention. Six isolated monogenetic scoria cones around the Lagoon Parihuana, scattered over a large area, with no tectonic relationship, are also obvious volcanic landforms in the “D cluster”.

The mineralogical and geochemical compositions of the analysed samples from the II-generation of the Andahua Group products show an increased degree of magma evolution (Figs. 8, 10 and 11). The rocks of this stage include both trachyandesites and more silicic derivatives – trachydacites, which petrographically indicate a transitional character between stages I and II. An increase in Rb content indicates a larger amount of continental crust contamination or can also occur by magma fractionation. The most contaminated melts are the silicic lavas from the Rio Molloco Valley (CM, C cluster, Appendix 2) and the Valley of the Volcanoes (ARCH1, A cluster, Appendix 2).

Based on the ratio of $^{206}Pb/^{204}Pb$ isotopes the Pampa Jarán volcanoes show clear influence of the Arequipa and Paracas domains (Figs. 12 and 13). Accordingly, on the north side of the Colca Canyon there is a transition zone (Mamani et al., 2010) bounded by the Puca Mauras volcano (AND-99-01, AND-99-10, Dealour et al., 2007) and the lava flows of the Sora Valley (APS4). The youngest products of such contamination cross the border of the transition zone marked by the Puca Mauras volcano and the lava flows in the Sora Valley. Everything indicates that the influence of the Gneiss Charcani as a contaminant is limited to the I of the Colca Canyon (Fig. 14).

Products from the Puca Mauras complex are more evolved compared to the other rocks of the AG and andraditic xenoliths are observed in the Huajana lava dome, that show mixed metamorphic-magmatic origin (Gałaś et al., 2021).

GENERATION III (10 KA–RECENT)

Numerous vents in the Valley of the Volcanoes (cluster A) and a single vent in both the Antapuna Massif (B cluster) and Huambo-Cabanaconde (G cluster) were formed in the past

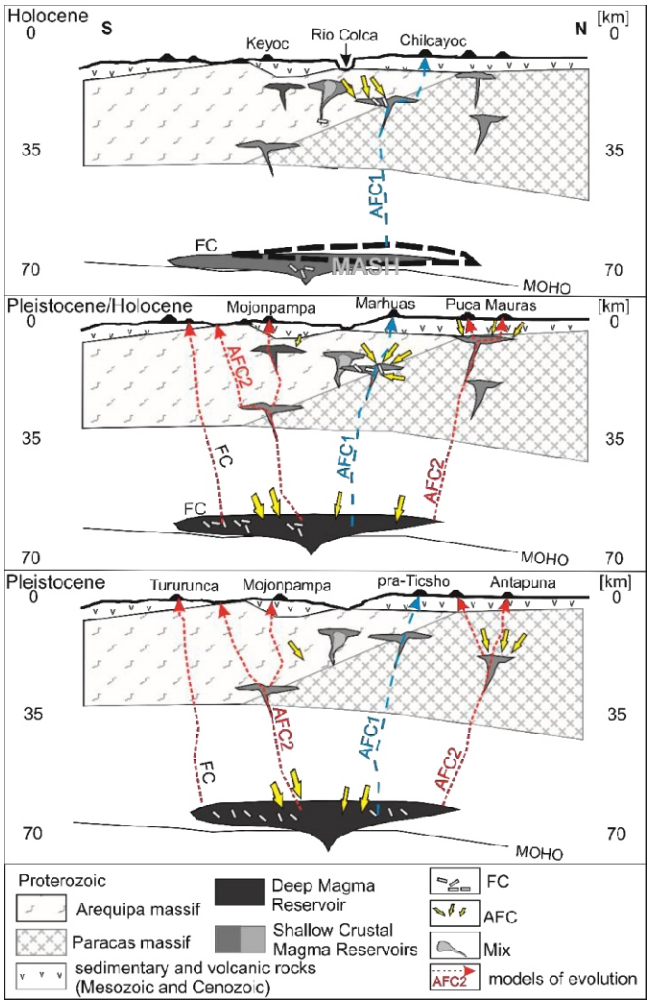

Fig. 14. Schematic development of the possible evolution of the AG magmatism

FC – fractional crystallization of olivines, clinopyroxenes and plagioclases; AFC – assimilation and fractional crystallization; Mix – magma mixing, MASH (Melting, Assimilation, Storage, Homogenization)

10 ka (Fig. 1C, Table 1, ^{14}C analysis by Cabrera and Thouret, 2000). The ^{14}C, K/Ar and U-series disequilibria analyses of products from this stage (Kaneoka and Gewarra, 1984; Delacour et al., 2007), provided eruption ages of 4050, 2900, 2650 and 520 years BP. For the Pumaranra lava domes, a relative eruption time of <10,000 years BP was determined (Bromley et al., 2019). Different volcanic materials from the Ticsho volcano (Fig. 2) were dated with the K/Ar method to 0.27 Ma and with ^{14}C to 4050 y BC (Kaneoka and Guevara, 1984; Cabrera and Thouret, 2000). The last dated eruption is the Chilcayoc Chico volcano 370 ±50 a (Cabrera and Thouret, 2000). A fresh lava surface and sparse vegetation coverage (Fig. 2) shows that the youngest volcanic landform is a Niñamama lava dome.

Only 9 lava domes and 9 scoria cones are recognized in total for this youngest generation. Three lava fields were formed in the Valley of the Volcanoes. They are (Fig. 2) the Chilcayoc, Sucna and Accompampa volcanoes. In the Chilcayoc field, initial outpouring points for lava flows are located at breached scoria cones such as the Chico, Chilcayoc and Chilcayoc Grande volcanoes. The Chico scoria cone is breached by a lava flow, and the edges of the older eruptive products are exposed in the walls of the main crater (Lewińska and Gałaś, 2021). The classic and regular monogenetic scoria cone of Jechapita has a small volume of 0.02 km^3 and probably stands at the top of a lava vent. The Chilcayoc lava field blocked the Andagua River, which created the Chachas Lagoon. The lava flows of this generation cover the southern part of the Valley of the Volcanoes from the line of Jenchaña-Niñamama connecting with the Colca Canyon. Lava domes and fissure vents feed the Accompampa and Sucna lava flow fields (Fig. 2). Two lava domes, near Sucna, emitted lava, which cascaded towards Colca Canyon. The highest of the lava domes is 70 m high and the longest lava flow is 20 km long. The small lava dome Niñamama is the typical form of the Andahua Group vents. The lava flow, out of the Niñamama lava dome is 4 km long, 1 km wide, and 33 m high, with a volume up to 0.25 km^3 (Figs. 2 and 5).

Lava flows of this generation show intermediate chemical character, and comprise only trachyandesites. They are also characterised by the highest ratio of $^{143}Nd/^{144}Nd$ (Gałaś, 2014). The geochemical and isotopic compositions (Appendix 3), and petrogenetic modelling, suggest reduced crustal contamination during this magmatic evolution stage. This probably indicates that an AFC1-type process was a dominant control for the evolution of this generation.

IMPLICATIONS FOR VOLCANIC HAZARD ASSESSMENT

During the Holocene 27 vents were active including 17 small lava domes or fissures and 8 scoria cones. They were located in clusters: A – Valley of the Volcanoes, B – Antapuna and G – Huambo-Cabanaconde (Fig. 1C). There are five scoria cones and two lava domes dated from 4050 to 370 years old (Cabrera and Thouret, 2000; Delacour et al., 2007). The activity zone is located between the Ticsho volcano in the north and the group of lava domes near Sucna in the south. The most likely region of volcanic reactivation is expected along three alignments of vents of previous Holocene eruption. In this area, the village of Andagua is located, the second most populated settlement in the Valley of the Volcanoes. Also in proximity are Chachas, Soporo and Sucna villages (Fig. 2).

Lava effusion and scoria eruption should be considered as a most likely eruption scenario for future volcanic activity. Strombolian style explosive activity is more hazardous than pure lava effusions (Vilches et al., 2022) due to the explosive nature of the former. The Andagua and Soporo settlements could suffer ashfall events as they are near to the sites of these expected future eruptions. The agricultural terraces around the villages would then be exposed both to falling volcanic bombs and tephra. Destruction of the areas and even temporary suspension of agricultural activity would deprive inhabitants of the settlements of their sole source of income.

All magmas contain dissolved gases that are released during effusive or extrusive type eruptions as well as between eruptive episodes. The agglomerates with andraditic garnet discovered on Huajana lava dome (Fig. 4) host numerous inclusions of anhydrite, halite, S- and Cl-bearing glass, anorthite, wollastonite and spinel (Gałaś et al., 2021). We speculate that volcanic activity of the Andahua Group might have produced substantial emission of sulphur in oxide and acidic form that could have caused formation of a volcanic fog that, in turn, might have been lethal (if concentrations of sulphur dioxide, hydrogen sulphide and sulphuric acid exceeded 20 ppm in air) to inhabitants or at least a source of irritation. This applies to two areas where evaporites are to be expected in the basement, i.e. Valley of the Volcanoes (cluster A) and Huambo-Cabanaconde (G).

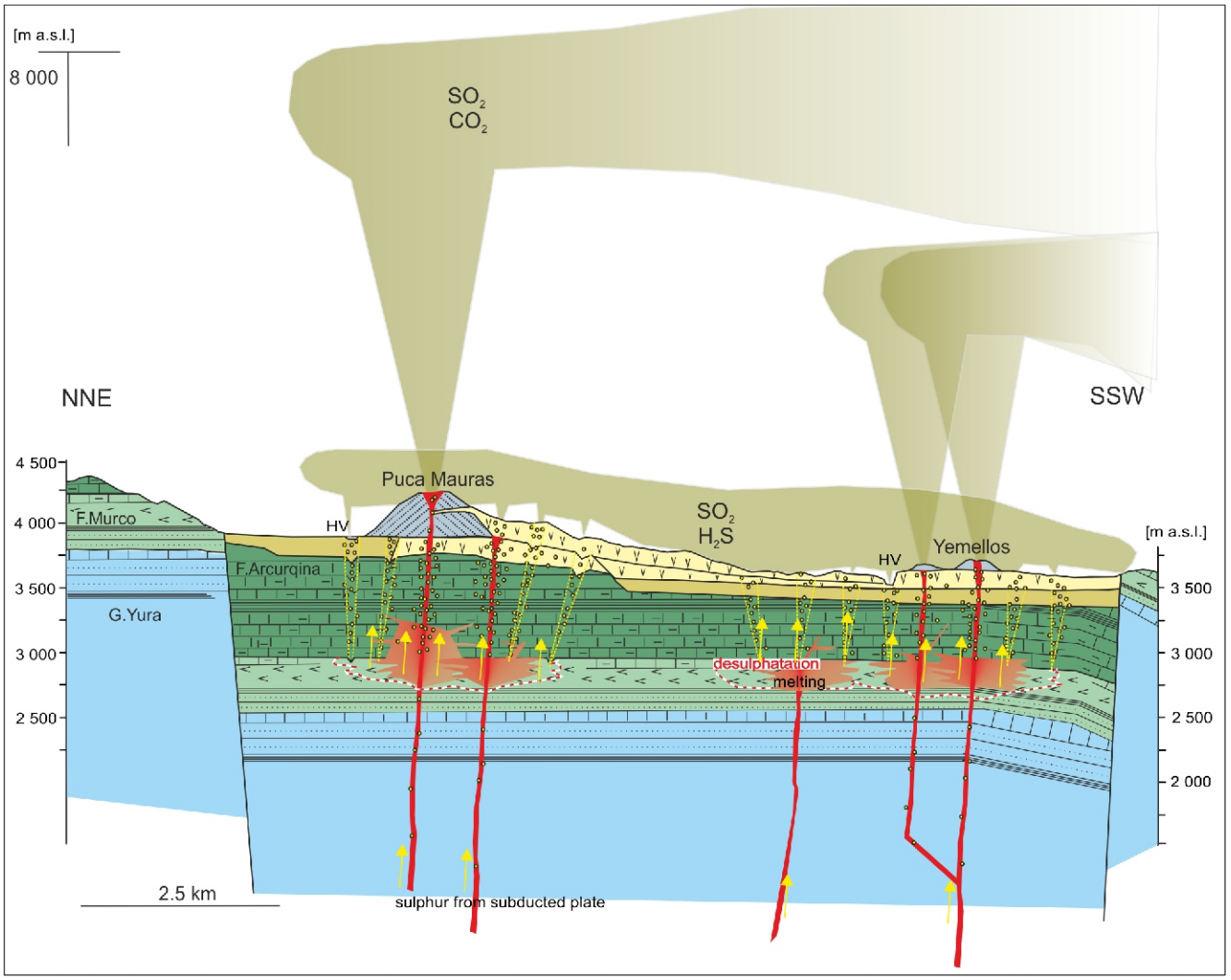

Fig. 15. Geological cross-section of the Puca Mauras volcano and possible scenario of the eruption with a cloud of toxic gases with a high content SO_2 and H_2S

There is no archaeological data on why the settlements of Antaymarca, Pajareta and Jello Jello in the valley were abandoned. Whether the abandonment resulted from the river being dammed causing disruption of the established irrigation system for agriculture, or the continuous degassing caused disease or even death, is still under debate. The possibility of an eruption is enhanced by the fact that exhalation of hydrogen sulphide was observed in the vicinity of the Niñamama dome in 2003 (Gałaś, 2011). Archive data and inclusions in crystals from the sustained lava eruption of the 1783–84 Laki Fissure in Iceland demonstrated that gas emissions were the direct and indirect cause of death on the island and in Europe (Thordarson et al., 2003; Gałaś, 2016). Just like the volcanoes of AG the Turrialba volcano (Costa Rica) also exhibited its latest activity with a maximum level of VEI 2. The volcano is dormant now but the continuous gas emission created a "death zone" in the immediate vicinity of the crater (Tortini et al., 2017). Initial research of sulphur-rich inclusions of garnet from AG lava indicates that wherever there are evaporites below ground, for example at Murco, Ashua and Huanca (Mayta et al., 2002), resumed volcanism can generate significant amounts of toxic gases (Gałaś et al., 2021). Therefore, even though volcanoes of the Andahua Group are inferred to have a low VEI, such eruptions have potential to pose a serious hazard to people and animals in the area (Fig. 15).

In the south, the Keyoc lava dome and the Mojonpampa lava field are ~10 km away from residential areas, hence the rejuvenation of volcanic eruptions from these regions would have lesser effect. The volcanic hazard that the Pumaranra vents can also pose is small due to the large distance between them and human settlements (Fig. 1C). The area, in the high Andes, is sparsely inhabited and underdeveloped, while the underground working silver mine of Arcata is separated by a mountain massif which would be a natural barrier against lava inundation or small scoria eruptions.

CONCLUSIONS

The minor volcanic centres of the Central Volcanic Zone, which are best represented by the Andahua Group volcanoes (149 centres), represent an extensive and variable magmatic history. Most of the volcanic centres are monogenetic, which means that the location of the eruption centres within a volcanic field changes their position over the lifespan of the system. Single eruption centres show the features of small complex forms.

The Andahua Group lavas compositionally range from basaltic andesites to trachydacite. The assumption that the volcanoes of the Andahua Group were fed from multiple magma reservoirs strongly limits the possibility of creating a single, consistent model for the evolution of the source magmas for this volcanic group. It also explains the relatively weak fit of magma evolution models developed by the authors and earlier workers. This situation results from an attempt to make models for the entire vent population, dispersed in both space and time. In this case, the change of the location of the volcanic activity is more important. This means that changes in the composition of the crustal rocks could influence small portions of magma that would consequently ascend in different ways. Very similar models are plausible for other monogenetic volcanoes of the Northern Andean segments, considering the possible effect of various compositions generated by crustal wall rock contamination on the ascending magmas (Murcia et al., 2019).

At substantial depths, a reservoir fed by a magma melted from a supra-subduction wedge in the presence of ascending fluids must have been formed. The low variability of the $^{87}Sr/^{86}Sr$ ratio suggests the presence of a single reservoir with a primitive magma. Conditions within the major, deep reservoir favoured the fractional crystallization of olivine, clinopyroxene and perhaps plagioclase. During the subsequent stages, some portions of magma were transported towards the surface, in these conditions crystallizing plagioclase, amphibole, and magnetite. The magmas were simultaneously contaminated to different degrees either by wallrocks in direct contact with the rising magmas, or by the rocks surrounding the reservoirs, i.e., the rocks of which the crystalline Paracas (AFC2) and Arequipa (AFC1) massifs are composed. Most of the samples show influence of the Paracas domain and is possible that the transition zone could be fed by magma reservoirs located exactly at the suture between the massifs, as suggested by Mamani et al. (2010). This means that there are two (or more) reservoirs, where magma is contaminated by different domains, or the same reservoir can be contaminated by one or the other massif. Processes involving the AFC2 and AFC1 models were the most significant. However, locally the fractional crystallization and Mix models can be inferred for the lavas.

The volcanoes of the Andahua Group are much smaller than the surrounding composite volcanoes. Their products show a much lower degree of source magma evolution. However, the same processes and magma regime are responsible for their creation. The pristine, extensive lava domes of Niñamama, and Pumaranra, and the scoria cones of Chico, and Chilcayoc Grande suggest that the Andahua Group is young (Pleistocene to Holocene) and potentially an active magmatic-volcanic system. The last activity at Chico occurred, at most, only 300 years ago. Long-lived Strombolian or Hawaiian type eruptions constitute a unique tourist attraction. All efforts should be made to ensure that such activity is under the watchful eye of specialists. Hence, it seems advisable to expand the monitored zone within the Valley of the Volcanoes similarly to other dispersed, potentially active volcanic fields such as the Auckland Volcanic Field in New Zealand (Hopkins et al., 2020). It is likely that gas emissions from the Andahua Group scoria cones and flood lava eruptions may create hazardous conditions for tourists visiting the Geopark Colca and Andagua Volcanoes in the case of future eruptions.

Acknowledgements. We thank H. Murcia for his constructive review of a previous version of this manuscript. We would like to thank J. Zalasiewicz for making English language corrections. The article was prepared under the research subvention of Polish Academy of Sciences and AGH University of Science and Technology, Kraków, Poland. Bulk rock chemical analyses were performed at ACTLABS Ltd. (Canada) on a commercial basis. NDVI analyses were performed by Ł. Nowak (AGH) in his master's thesis.

REFERENCES

Aitcheson, S.J., Forrest, A.H., 1994. Quantification of crustal contamination in open magmatic systems. Journal of Petrology, **35**: 461–488.

Anderson, A., Greenland, L.P., 1969. Phosphorus fractionation diagrams as a quantitative indicator of crystallization differentiation of basaltic liquids. Geochimica et Cosmochimica Acta, **33**: 493–505.

Baker, M., Wyllie, P.J., 1992. High-pressure apatite solubility in carbonate-rich liquids – implication for mantle metasomatism. Geochimica et Cosmochimica Acta, **56**: 3409–3422.

Beck, S., Zandt, G., Myers, S.L., Wallace, T., Silver, P., Drake, L.P., 1996. Crustal thickness variations in the Central Andes. Geology, **24**: 407–410.

Borrero, C., Murcia, H., Agustín-Flores, J., Arboleda, M.T., Giraldo, A.M., **2017**. Pyroclastic deposits of San Diego Maar, central Colombia: an example of a silicic magma related monogenetic eruption in a hard substrate. Geological Society Special Publications, **446**: 361–374.

Botero-Gómez, L.A., Osorio, P., Murcia, H., Borrero, C., Grajales, J.A., 2018. The Villamaria-Termales Monogenetic Volcanic Field, Central Cordillera, Colombian Andes (Part I): Morphological features and temporal relationships. Boletin De Geologia, **40**: 85–102.

Bromley, G.R.M., Thouret, J., Schimmelpfennig, I. Mariño, J., Valdivia, D., Rademaker, K., del Pilar, V.L.S., ASTER Team, Aumaître, G., Bourlès, D., Keddadouche, K., 2019. In situ cosmogenic ^{3}He and ^{36}Cl and radiocarbon dating of volcanic deposits refine the Pleistocene and Holocene eruption chronology of SW Peru. Bulletin of Volcanology, **81**, 64.

Cabrera, A.P., Caffe P.J., 2009. The Cerro Morado andesites; volcanic history and eruptive styles of a mafic volcanic field from northern Puna, Argentina. Journal of South American Earth Sciences, **28**: 113–131.

Cabrera, M., Thouret, J.C., 2000. Volcanismo monogenético en el sur del Perú. X Congr Peruano de Geol. Sociedad Geológica del Perú, Lima.

Caldas, J., La Torre, V., Lajo, A., Díaz, J., Umpire, L., 2001. Mapa geológico del cudrángulo de Orcopampa (actualizado) 1:100,000. INGEMMET, Peru.

Davidson, J.P., de Silva, S.L., 1995. Late Cenozoic magmatism of the Bolivian Altiplano. Contributions to Mineralogy and Petrology, **119**: 387–408.

Delacour, A., Gerbe, M.Ch., Thouret, J.C., Wörner, G., Paquereau-Lebti, P., 2007. Magma evolution of Quaternary minor volcanic centres in southern Peru, Central Andes. Bulletin of Volcanology, **69**: 581–608.

Delph, J.R., Ward, K.M., Zandt, G., Ducea, M.N., Beck, S.L., 2017. Imaging a magma plumbing system from MASH zone to magma reservoir. Earth and Planetary Science Letters, **457**: 313–324.

De Paolo, D.J., 1981. Trace-element and isotopic effects of combined wallrock assimilation and fractional crystallization. Earth and Planetary Science Letters, **53**: 189–202.

De Silva, S.L., Francis, P.W., 1991. Volcanoes of the Central Andes. Springer, Berlin, Heidelberg.

De Silva, S.L., Kay S.M., 2018. Turning up the heat: high-flux magmatism in the Central Andes. Elements, **14**: 245–250.

Dewey, J., Lamb, S., 1992. Active tectonics of the Andes. Tectonophysics, **205**: 79–95.

Dóniz-Páez, J., Romero-Ruiz, C., Sánchez, N., 2012. Quantitative size classification of scoria cones: the case of Tenerife (Canary Islands, Spain). Physical Geography, **33**: 514–535.

Eash, N.S., Sandor, J.A., 1995. Soil chronosequence and geomorphology in a semi-arid valley in the Andes of southern Peru. Geoderma, **65**: 59–79.

England, P., Engdahl, R., Thatcher, W., 2004. Systematic variation in the depths of slabs beneath arc volcanoes. Geophysical Journal International, **156**: 377–40.

Fink, J.H., Griffiths, R.W., 1998. Morphology, eruption rates, and rheology of lava domes: Insights from laboratory models. Journal of Geophysical Research-Solid Earth, **103** (B1): 527–545.

Fornaciai, A., Favalli, M., Karátson, D., Tarquini, S., Boschi, E., 2012. Morphometry of scoria cones, and their relation to geodynamic setting: A DEM-based analysis. Journal of Volcanology and Geothermal Research, **217–218**: 56–72.

Francis, P., Oppenheimer, C. 2004. Volcanoes. Oxford University Press, Second edition.

Gałaś, A., 2011. The extent and volcanic structures of the Quaternary Andahua Group, Andes, southern Peru. Annales Societatis Geologorum Poloniae, **81**: 1–19.

Gałaś, A., 2013. The characteristics of the Andahua Volcanic Group in southern Peru (in Polish with English summary). AGH University of Science and Technology Press, Dissertations, Monographs, **281**.

Gałaś, A., 2014. Petrology and new data on the Geochemistry of the Andahua Volcanic Group (Central Andes, southern Peru). Journal of South American Earth Sciences, **56**: 301–315.

Gałaś, A., 2016. Impact of volcanic eruptions on the environment and climatic conditions in the area of Poland (Central Europe). Earth-Science Reviews, **162**: 58–64.

Gałaś, A., Gałaś, S., 2017. Conditions of development of volcanic attractions in the planned Colca and Andagua Volcanoes Geopark in Southern Peru. Conference: Public recreation and landscape protection – with hand in hand…, Department of Landscape Management FFWT, Mendel University in Brno, 1–3 may: 63–68.

Gałaś, A., Paulo, A., Gaidzik, K., Zavala, B., Kalicki, T., Churata, D., Gałaś, S., Mariño, J., 2018. Geosites and geotouristic attractions proposed for the project Geopark Colca and Volcanoes of Andagua, Peru. Geoheritage, **10**: 707–729.

Gałaś, A., Majka, J., Włodek, A., 2021. Origin of andradite in the Quaternary volcanic Andahua Group, Central Volcanic Zone, Peruvian Andes. Mineralogy and Petrology, **115**: 257–269.

Gerbe, M.Ch., Thouret, J.C., 2004. Role of magma mixing in the petrogenesis of tephra erupted during the 1990–98 explosive activity of Nevado Sabancaya, southern Peru. Bulletin of Volcanology, **66**: 541–561.

Gill, J.B. 1981. Orogenic andesites and plate tectonics. Springer, Berlin-Heidelberg-New York.

Godoy, B., Wörner, G., Kojima S., Auguilera, F., Simnon, K. 2014. Low-presure evolution of arc magmas in thickened crust: the San Pedro-Linzor volcanic chain, Central Andes, northern Chile. Journal of South American Earth Sciences, **52**: 24–42.

González, A., Fernández-Turiel, J.L., Pérez-Torrado, F.J, Aulinas, M.C., Hervé, D.G., 2011. GIS methods applied to the degradation of monogenetic volcanic fields: a case study of the Holocene volcanism of Gran Canaria (Canary Islands, Spain). Geomorphology, **134**: 249–259.

Gutiérrez, F., Gioncada, A., Ferran, O.G., Lahsen, A., Mazzuoli, R., 2005. The Hudson Volcano and surrounding monogenetic centres (Chilean Patagonia): an example of volcanism associated with ridge-trench collision environment. Journal of Volcanology and Geothermal Research, **145**: 207–233.

Guzmán, S.R., Petrinovic, I.A., Brod, J.A., 2006. Pleistocene mafic volcanoes in the Puna-Cordillera Oriental boundary, NW-Argentina. Journal of Volcanology and Geothermal Research, **158**: 51–69.

Haag, M.B., Báez, W.A., Sommer, C.A., Arnosio, J.M., Filipovich, R.E., 2019. Geomorphology and spatial distribution of monogenetic volcanoes in the southern Puna Plateau (NW Argentina). Geomorphology, **342**: 196–209.

Hawkesworth, C., Clarke, C., 1994. Partial melting in the Lower crust: new constraints on crustal contamination processes in the Central Andes. In: Tectonics of the Southern Central Andes, Structure and Evolution of an Active Continental Margin (eds. K.J. Reutter, E. Scheuber and P.J. Wigger): 93–101. Springer, Berlin.

Hopkins, J.L., Smid, E.R., Eccles, J.D., Hayes, J.L., Hayward, B.W., McGee, L.E., van Wijk, K., Wilson, T.M., Cronin, S.J., Leonard, G.S., Lindsay J.M., Németh, K., Smith I.E.M., 2020. Auckland Volcanic Field magmatism, volcanism, and hazard: a review. New Zealand Journal of Geology and Geophysics, **64**: 1–22.

Huang, F., Sørensen, E.V., Holm, P.M., Zhang, Z.F., Lundstrom, C.C., 2017. U-series disequilibria of trachyandesites from minor volcanic centers in central Andes. Geochimica et Cosmochimica Acta, **215**: 92–104.

Huete, A.R., 1988. A soil-adjusted vegetation index (SAVI). Remote Sensing of Environment, **25**: 295–309.

James, D.E., 1982. A combined O, Sr, Nd and Pb isotopic and trace element study of crustal contamination in central Andean lavas. Earth and Planetary Science Letters, **57**: 47–62.

James, D.E., Brooks, Ch., Cuyubamba, A., 1976. Andean Cenozoic volcanism: magma genesis in the light of strontium isotopic composition and trace element geochemistry. GSA Bulletin, **87**: 592–600.

Janoušek, V., Moyen, J.-F., Martin, H., Erban, V., Farrow, C., 2015. geochemical modelling of igneous processes: Principles and recipes in R language. Bringing the power of R to a geochemical community. Springer Geochemistry, Berlin and Heidelberg.

Jensen, J.R., 1986. Introductory Digital Image Processing: A Remote Sensing Perspective. Prentice-Hall, Englewood Cliffs, New Jersey.

Kaneoka, I., Guevara, C., 1984. K-Ar determinations of late Tertiary and Quaternary Andean volcanic rocks, Southern Peru. Geochemical Journal, **18**: 233–239.

Kay, S.M., Godoy, E., Kurtz, A., 2005. Episodic arc migration, crustal thickening, subduction erosion, and magmatism in the south-central Andes. GSA Bulletin, **117**: 67–88.

Kereszturi, G., Németh, K., 2011. Shallow-seated controls on the evolution of the Upper Pliocene Kopasz-hegy nested monogenetic volcanic chain in the Western Pannonian Basin (Hungary). Geologica Carpathica, **62**: 535–546.

Klerkx, J., Deutsch, S., Pichler, H., Zeil, W., 1979. Strontium isotopic and trace element data bearing on the origin of Cenozoic volcanic rocks of the Central and Southern Andes). Journal of Volcanology and Geothermal Research, **2**: 49–71.

La Maitre, R.W., Bateman, P., Dudek, A., Keller, J., Lameyre, J., Le Bas, M., Sabine, P.A., Schmid, R., Sřrensen, H., Streckeisen, A., Wooley, A.R., Zanettin, B., 1989. A classification of igneous rocks and glossary of terms: recommendations of the International Union of Geological Sciences Subcommission on the Systematics of Igneous Rocks. Blackwell Scientific Publications, Oxford.

Lewińska P., Gałaś, A., 2021. Use of structure-from-motion algorithms for geomorphological analyses of simple volcanic structures: A case study of Chilcayoc Chico and four other volcanoes of the Andahua Group, Peru. Journal of South American Earth Sciences, **107**, https://doi.org/10.1016/j.jsames.2020.103058

Lewińska, P., Glowacki, O., Moskalik, M., Smith, W.A.P., 2021. Evaluation of structure-from-motion for analysis of small-scale glacier dynamics. Measurement, **168**, https://doi.org/10.1016/j.measurement.2020.108327

Lucassen, F., Becchioc, R., Harmond, R., Kasemanna, S., Franza, G., Trumbulle, R., Wilkef, H.G., Romere, R.L., Dulskie, P., 2001. Composition and density model of the conti-

nental crust at an active continental margin – the Central Andes between 21° and 27°S. Tectonophysics, **341**: 195–223.

Maciuk, K., 2016. Different approaches in GLONASS orbit computation from broadcast ephemeris. Geodetski vestnik, **60**: 437–448.

Mali, V.K., Kuiry, S.N., 2018. Assessing the accuracy of high-resolution topographic data generated using freely available packages based on SfM-MVS approach, Meas. Journal of the International Measurement Confederation, **124:** 338–350.

Mamani, M., Tassara, A., Wörner, G., 2008. Composition and structural control of crustal domains in the Central Andes. Geochemistry, Geophysics, Geosystems, **9**: 1–13.

Mamani, M., Wörner, G., Sempere, T., 2010. Geochemical variations in igneous rocks of the Central Andean orocline (13°S to 18°S): Tracing crustal thickening and magma generation through time and space. GSA Bulletin, **22**: 162–182.

Mattsson, H.B., Hoskuldsson, A., 2005. Eruption reconstruction, formation of flow-lobe tumuli and eruption duration in the 5900 BP Helgafell lava field (Heimaey), south Iceland. Journal of Volcanology and Geothermal Research, **147**: 157–172.

Mayta, O., Barrionuevo, H., Noble, D., Petersen, U., Vidal, C., 2002. Vetas de oro nativo y telururos de oro en el sector Chipmo, distrito minero de Orcopampa, sur del Perú. XI Congreso Peruano de Geología. Boletin Sociedad Geológica del Perú, Lima.

Murcia, H., Borrero, C., Németh, K., 2019. Overview and plumbing system implications of monogenetic volcanism in the northernmost Andes' volcanic province. Journal of Volcanology and Geothermal Research, **383**: 77–87.

Németh, K., Haller, M.J., Martin, U., Risso, C., Massaferro, G., 2008. Morphology of lava tumuli from Mendoza (Argentina), Patagonia (Argentina), and Al-Haruj (Libya). Zeitschrift für Geomorphologie, **52**: 181–194.

Niipele, J.N., Chen, J., 2019. The usefulness of ALOS-PALSAR DEM data for drainage extraction in semi-arid environments in the Iishana sub-basin. Journal of Hydrology: Regional Studies Volume, **21**: 57–67

Park, H., Lee, D., 2019. Comparison between point cloud and mesh models using images from an unmanned aerial vehicle, Meas. Journal of the International Measurement Confederation, **138**: 461–466.

Petrelli, M., Poli, G., Perugini, D., Peccerillo, A., 2005. Petrograph: a new software to visualize, model, and present geochemical data in igneous petrology. Geochemistry, Geophysics, Geosystems, **6:** Q07011.

Ramos, V.A., 2008. The basement of the Central Andes: the Arequipa and related terranes. Annual Review of Earth and Planetary Sciences, **36**: 289–324.

Reynolds, P., Brown, R.J., Thordarson, T., Llewellin, E.W., 2016. The architecture and shallow conduits of Laki-type pyroclastic cones: insights into a basaltic fissure eruption. Bulletin of Volcanology, **78**: 36.

Ringwood, A.E., 1974. Petrological evolution of island arc systems. Journal of the Geological Society, London, **130**: 183–204.

Rogers, N., Hawkesworth, C., 2000. Composition of magmas. In: Encyclopedia of Volcanoes (eds. H. Sigurdsson, B.F. Houghton, S.R. McNutt, H. Rymer and J. Stix): 115–131. Academic Press, San Diego.

Rollinson, H.R., 1993. Using Geochemical Data: Evaluation, Presentation, Interpretation. Longman Scientific and Technical.

Romanyuk, T.V., 2009. The Late Cenozoic geodynamic evolution of the central segment of the Andean subduction zone. Geotectonics, **43**: 305–323.

Ruprecht, P., Wörner, G., 2007. Variable regimes in magma systems documented in plagioclase zoning patterns: El Misti stratovolcano and Andahua monogenetic cones. Journal of Volcanology and Geothermal Research, **165**: 142–162.

Salas, P.A., Rabbia, O.M., Hernández, L.B., Ruprecht, P., 2017. Mafic monogenetic vents at the Descabezado Grande volcanic field (35.5°S–70.8°W): the northernmost evidence of regional primitive volcanism in the Southern Volcanic Zone of Chile. International Journal of Earth Sciences, **106**: 1107–1121.

Samaniego, P., Rivera, M., Mariño, J., Guillou, H., Liorzou, C., Zerathe, S., Delgado, R., Valderrama, P., Scao, V., 2016. The eruptive chronology of the Ampato–Sabancaya volcanic complex (Southern Peru). Journal of Volcanology and Geothermal Research, **323**: 110–128.

Sánchez-Torres, L., Toro, A., Murcia, H., Borrero, C., Delgado, R., Gómez-Arango, J., 2019. El Escondido tuff cone (38ka): a hidden history of monogenetic eruptions in the northernmost volcanic chain in the Colombia Andes. Bulletin of Volcanology, **81**: 71.

Sánchez-Torres, L., Murcia, H., Schonwalder-Ángel, D., 2022. The northernmost volcanoes in South America (5–6°N): the potentially active Samaná Monogenetic Volcanic Field. Frontiers in Earth Science, **943**: 23.

Schiano, P., Monzier, M., Eissen, J.-P., Martin, H., Koga, K.T., 2010. Simple mixing as the major control of the evolution of volcanic suites in the Ecuadorian Andes. Contributions to Mineralogy and Petrology, **160**: 297–312.

Sébrier, M., Soler, P., 1991. Tectonics and magmatism in the Peruvian Andes from late Oligocene time to Present. GSA Special Papers, **265**: 259–278.

Smoll, F.L., Morche, W., Nuñez, J.S., 1997. Inventario de volcanes del Peru. INGEMMET Lima, Boletin, **15**.

Somoza, R., 1998. Update Nazca (Farallon) – South America relative motions during the last 40 Ma: implications for the mountain building in the Central Andean region. Journal of South American Earth Sciences, **11**: 211–215.

Sørensen, E.V., Holm, P.M., 2008. Petrological inferences on the evolution of magmas erupted in the Andagua Valley, Peru (Central Volcanic Zone). Journal of Volcanology and Geothermal Research, **177**: 378–396.

Stern, C.R., 2004. Active Andean volcanism: its geologic and tectonic setting. Revista Geologica de Chile, **31**: 161–206.

Störmer, J.-C., Nicholls, J., 1978. XIfrac: a program for the interactive testing of magmatic differentiation models. Computers and Geosciences, **4**: 143–159.

Sun, S.S., Mc Donough, W.F., 1989. Chemical and isotopic systematics of oceanic basalts: implications for mantle composition and processes. Geological Society Special Publications, **42**: 313–345.

Swanson, E., Noble, D., Connors, K., Mayta, O., Mckee, E., Sánchez, A., Heizler, M., 2004. Mapa geológico del cuadrángulo de Orcopampa (Sur del Perú). INGEMMET Lima, Boletín, Serie A: Carta Geológica Nacional, **137.**

Tadono, T., Ishida, H., Oda, F., Naito, S. , Minakawa, K., Iwamoto, H., 2014. "Precise global DEM generation by ALOS PRISM," ISPRS Annals of the Photogrammetry, Remote Sensing and Spatial Information Sciences, Volume II-4, 2014, ISPRS Technical Commission IV Symposium, 14–16 May, 2014, Suzhou, China, URL: http://www.isprs-ann-photogramm-remote-sens-spatial-inf-sci.net/II-4/71/2014/isprsannals-II-4-71-2014.pdf

Tepley, F.J, de Silva, S., Salas, G., 2013, Magma dynamics and petrological evolution leading to the VEI 5 2000 BP eruption of El Misti volcano, southern Peru. Journal of Petrology, **54**: 2033–2065.

Thordarson, Th., Self, S., Oskarsson, N., Hulsebosch, T., 1996. Sulfur, chlorine, and fluorine degassing and atmospheric loading by the 1783–1784 AD Laki (Skaftár Fires) eruption in Iceland. Bulletin Volcanology, **58**: 205–225.

Thorpe, R.S., Francis, P.W., 1979. Variations in Andean andesite compositions and their petrogenetic significance. Tectonophysics, **57**: 53–70.

Thorpe, R.S., Francis, P.W., O'Callaghan, L., 1984. Relative roles of source composition, fractional crystallization and crustal contamination in the petrogenesis of Andean volcanic rocks. Philosophical Transactions of the Royal Society of London, **310**: 675–692.

Thouret, J.C., Jicha, B.R., Paquette, J.L., Cubukcu, E.H., 2016. A 25 myr chronostratigraphy of ignimbrites in south Peru: implications for the volcanic history of the Central Andes. Journal of Geological Society, **173**: 734–756.

Tortini, R., van Manen, S.M., Parkes, B.R.B., Carn, S.A., 2017. The impact of persistent volcanic degassing on vegetation: A case

study at Turrialba volcano, Costa Rica. International Journal of Applied Earth Observation and Geoinformation, **59**: 92–103.

Trumbull, R.B., Wittenbrink, R., Hahne, K., Emmermann, R., Büsch, W., Gerstenberger, H., Siebel, W., 1999. Evidence for late Miocene to Recent contamination of arc andesites by crustal melts in the Chilean Andes (25–26°S) and its geodynamic implications. Journal of South American Earth Sciences, **12**: 135–155.

Ureta, G., Németh, K., Aguilera, F., Kósik, S., 2019. Cinder cones of the Quaternary Ollagüe Volcanic Field, Central Andean Volcanic Zone, northern Chile. IAVCEI – 5th International Volcano Geology Workshop Palmerston North, New Zealand, 2019, abstract.

Ureta, G., Németh, K., Aguilera, F., González, R., 2020. Features That favor the prediction of the emplacement location of maar volcanoes: a case study in the Central Andes, Northern Chile. Geosciences, **10**.

Wessling, R.B., 1999. The SRTM Mission: A World-Wide 30 m Resolution DEM from SAR in 11 days, Photogrammetric week '99, https://phowo.ifp.uni-stuttgart.de/publications/phowo99

Wilson, B.M., 1989. Igneous Petrogenesis a Global Tectonic Approach. Springer.

Wörner, G., Mamani, M., Blum-Oeste, M., 2018. Magmatism in the Central Andes. Elements, **14**: 237–244.

Vespermann, D., Schmincke, H.-U., 2000. Scoria cones and tuff rings. In: Encyclopedia of Volcanoes (eds. H. Sigurdsson, B.F. Houghton, S.R. McNutt, H. Rymer and J. Stix): 683–694. Academic Press, San Diego.

Yuan, X., Sobolev, S.V., Kind, R., 2002. Moho topography in the Central Andes and its geodynamic implication. Earth and Planetary Science Letters, **199**: 389–402.

Zavala, B., Churata, D., 2016. Colca y Volcanes de Andagua Geopark, Arequipa, Perú: application dossier for nomination as geopark. Geological Heritage, Document process for UNESCO Global Geoparks aspiring, information prepared by INGEMMET. PALSAR_Radiometric_Terrain_Corrected_high_res, Alaska Satellite Facility (ASF) Distributed Active Archive Center (DAAC), doi: 10.5067/Z97HFCNKR6VA

APPENDIX 1

Representative analyses used as inputs for petrological modelling

Sample	vol6*	BAS 21**	OCO0708**	OCO0703**
Oxide contents (wt.%):				
SiO_2	51.43	67.1	61.77	69.97
TiO_2	1.21	0.5	1.1	0.63
Al_2O_3	16.71	15.4	22.73	13.24
Fe_2O_3	9.03	4.09	7.81	4.2
MnO	0.12	0.07	0.09	0.08
MgO	7.30	1.87	1.73	1.02
CaO	8.72	3.44	0.26	1.89
Na_2O	3.37	3.62	0.4	3.21
K_2O	1.38	2.63	3.15	4.29
P_2O_5	0.29	0.14	0.04	0.21
LOI	0.38	n.d.	n.d.	n.d.
Total	99.94	n.d.	n.d.	n.d.
Trace elements (ppm):				
Nb	5	9	24.8	11.7
Ti	7260	n.d.	n.d.	n.d.
Zr	137	161	327	287
Th	2.21	1.5	24.1	7.9
La	19.54	30.8	76	49
Cr	372	30	114	9
Ni	134	20	54	12
V	215	67	107	58
P	1763	n.d.	n.d.	n.d.
$^{87}Sr/^{86}Sr$	0.7067	0.7303	0.7076	0.7242
$^{143}Nd/^{144}Nd$	0.5124	0.5115	0.5115	0.5117
Sample	vol6*	BAS 21**	OCO0708**	OCO0703**
Oxide contents (wt.%):				
SiO_2	51.43	67.1	61.77	69.97
TiO_2	1.21	0.5	1.1	0.63
Al_2O_3	16.71	15.4	22.73	13.24
Fe_2O_3	9.03	4.09	7.81	4.2
MnO	0.12	0.07	0.09	0.08
MgO	7.30	1.87	1.73	1.02
CaO	8.72	3.44	0.26	1.89
Na_2O	3.37	3.62	0.4	3.21
K_2O	1.38	2.63	3.15	4.29
P_2O_5	0.29	0.14	0.04	0.21
LOI	0.38	n.d.	n.d.	n.d.
Total	99.94	n.d.	n.d.	n.d.
Trace elements (ppm):				
Nb	5	9	24.8	11.7
Ti	7260	n.d.	n.d.	n.d.
Zr	137	161	327	287
Th	2.21	1.5	24.1	7.9
La	19.54	30.8	76	49
Cr	372	30	114	9
Ni	134	20	54	12
V	215	67	107	58
P	1763	n.d. 0.7303	n.d. 0.7076	n.d. 0.7242
$^{87}Sr/^{86}Sr$	0.7067	0.5115	0.5115	0.5117
$^{143}Nd/^{144}Nd$	0.5124			

* – Delacour et al. (2007); ** – Mamani et al. (2008); n.d. – not detected

APPENDIX 2

Lava dome and lava vents of the Andahua Group

(Smoll et al., 1997; Gałaś, 2011)

No.	Cluster	Name/ sample	GPS position	Generation/ age	Type
1	A. The Valle the of the Volcanoes	IS1	784855 8286570	I 0.5 Ma*	unrecognized
2		An	–	I	unrecognized
3		D10	76282 86137	I	1A
4		DK8	–	I	1A
5		VCO (VCO)	780727 283914	I	1A
6		VCO II	780727 283914	I	1A
7		VCO1	780819 283754	I	1A
8		VCO3	780821 283576	I	1A
9		TK2 (TK2)	82534 86490	I	1A
10		T3	782105 287631	I	1C
11		Pra Ticscho/PT	0781375 8286482	I 0.27 Ma*	1C
12		PT1	–	I	1B
13		Soporo	–	I	unrecognized
14		Tororocsa	7878 82987*	I	unrecognized
15		Jullulluyoc	7810 83142*	I	unrecognized
16		A13 (A13)	–	I/II	unrecognized
17		A131 (A14)	–	I/II	unrecognized
18		Cerros Umajala	–	I/II	1B
19		Cerro Anchajolla	–	II	1A
20		Chipchane (ARCH1)	786157 290311	II	1C
21		V8B	–	II	1C
22		V8C	–	II	1B
23		V8D	–	II	1B
24		V8E	–	II	1A
25		MS2	–	II	1A
26		MS5	–	II	1A
27		MS6	–	II	1B
28		MS7	–	II	1B
29		C. Ashillo	–	II	1A
30		LS	–	II	1A
31		Cochapampa (C1A)	0782708 8284695	II	1C
32		Jochane	7734 83065*	II	1C
33		MS1 (MS1)	772820 311670	II	1A
34		APS4			
35		A6	785639 283277	III	1A
36		Ninamama (A7)	0786545 8284465	III	1A
37		Antaymarca	0784608 8282862	III	1B
38		A26	784971 282792	III	1B
39		Accopampa	–	II	1B
40		J2	–	III	1B
41		S61	–	III	1B
42		S62	–	III	1B
43	B. Antapuna	Cerro Antapuna (Anta2)	0779944 8322476	I	unrecognized
44		Tanca	–	I	unrecognized
45		PP1	–	I	1A
46		PP2	–	I	1A
47		AR2 (AR2)	0800936 8335962	I	
48		Pumaranra (Pum1)	783680 8340670	III	1A
49	C. Rio Molloco	Cerro Coropuna (CM)	814057 287241	II	Pelean
50		C	–	I	unrecognized
51		T	–	I	unrecognized
52		CM1	–	II	1A
53		M1	–	II	1A
54		M2	–	II	1A
55		M3	–	II	1A
56		M4	–	II	1A
57		U2	–		1A
58		Uchuychaca	1814 82863*	II	1A
59	E. Valley of Rio Colca	Cano 1	224651 8277959	I	unrecognized
60		Can1 (CAN1)	224605 8277815	I	unrecognized
61		Chi2	220737 8270021	I	unrecognized
62		Cal3	222305 8271721	I	unrecognized
63		Lari2 (LARI12)	203782 8269446	I	unrecognized
64		Cal2 (CAL2)	221640 8271073	I/II 172 ka BP i 64 ka BP, 0.23 Ma**	1C
65		OC4 (CC4)	220584 274741	II	1B
66		OC2 (OC1)	220368 275337	II 0.095 Ma*	1B
67		OC5	220643 273977	II	1B
68		Can5 (CAN5)	223263 8275703	II	1B
69		Can6	223355 8275064	II	1B
70	F. Jaran	P010 (H010)	806254 8247247	I	1A
71		P011	–	I	1A
72		P012	–	I	1A
73		CP5	802582 8242444	I	1A
74		MG1	0802312 8243872	I	1A
75		MBK2	807907 243918	I	1B
76		MBK21	–	I	1B
77		MBK22	–	I	1B
78		GL9	792253 8244556	I	unrecognized
79		GL4	794679 242847	I	unrecognized
80		GL91 (GU12)	–	I	unrecognized
81		H45	807552 8233126	I	unrecognized
82		Q1	–	I	unrecognized
83		Q2 (Pe1)	–	I	unrecognized
84	G. Huambo–Cabanaconde	MOK3	814738 263255	I	unrecognized
85		MOK4	815035 262907	I	unrecognized
86		SO6	810654 265835	I	unrecognized
87		UP1	810447 268128	I	1A
88		SO8	811553 269382	I	1B
89		SO11	–	I	1B
90		SO12	–	I	1B
91		FU5	–	I	1A
92		FU6	–	I	1A
93		SO21 (LE3)	–	I	1A
94		LE1	815085 268021	I	1A

95		FU2	813120 268292	I	1A
96		FU3	813282 268291	I	unrecognized
97		FU4	813640 268348	I	unrecognized
98		014	814695 8261821	I	unrecognized
99		015 (H015b)	815065 8261593	I	unrecognized
100		MJ3	819671 262627	II	unrecognized
101		MJ32	–	II	1B
102		Jajacuchu (HU2)	0807944 8258557	II	1A
103		HU21	–	II	1A
104		Keyoc		III 2650 year BP*	1A

GPS position: * – Smoll et al. (1997); age: * – Cabrera and Thouret (2000); ** – Eash and Sandor (1995)

Scoria cone and composite volcanoes of Andahua Group

(Smoll et al., 1997; Gałaś, 2011)

No.	Cluster	Name/Sample	GPS position	Generation/Age	Type
1	A. The Valle the of the Volcanoes	Panahua	787695 8298546	I	2A
2		Ucuya (AC3)	785312 281913	I	2B
3		Pampalquita (CM2)	7884506 281307	I	2B
4		Yanamauras Sur	783910 8286304	II	2A
5		Yanamauras	784214 8286652	II	2A
6		eroded	783956 8287271	II	unrecognized
7		Cerro Puca Mauras	785722 8293030	II	small composite
8		Cerro Mauras	787022 8302521	II	2C
9		Santa Rosa	7875 82945*	II	2A
10		Santa Rosa Sur	7867 82934*	II	2A
11		Challhue Mauras	7847 82998*	II	2A
12		Misahuana Mauras (V9a, V9b)	770325 8311264	II	2A
13		Pabellon Mauras	7729 83084*	II	2A
14		Yana Mauras (YM1)	775612 8305161	III 2900 year BP**	2A
15		Ticsho	781375 8286482	III 4050 year*	2C
16		Mauras (Mau2)	7840 83124*	III 2900 year BP**	2A
17		Jenchaña	784664 8282346	III	2C
18		Jechapita (J1)	788499 8280856	III	2A
19		Chilcayoc Grande (CH2S)	790847 8280756	III A.D. 1500**	2A
20		Chilcayoc	788139 8282003	III	2B
21		Chilcayoc Chico	787693 8282304	III 370 ±50 year ago*	2BC
22		Cerro Pucamauras	7974 82898*	I	2A
23		Cerro Ticlla	No data	I	unrecognized
24	B. Antapuna	Cerro Antopuna	788955 8323619	I	small composite
25		Cerro Antapuna	791296 8322876	I	parasitic?
26		Ares I	804174 8333531	II	unrecognized
27		Ares II	800936 8335962	II	unrecognized
28	C. Molloco	Marhuas (VM21)	800936 8335962	II	2A
29	D. Laguna Parihuana	Antaymarca (HT1)	196077 8306538	60,000 year*** II	2A
30		Saigua	2004 83136*	II	unrecognized
31		Challpo	2000 83075*	II	unrecognized
32		Andallullo	1980 82976*	II	unrecognized
33		Antaccollo	2098 83049*	II	unrecognized
34		Sani	2095 82954*	II	unrecognized
35	F. Jaran	Gloriahuasi (H58)	792860 8243760	I	small composite
36		Gloriahuasi Sur (GL8)	791856 8242754	I	
37		San Cristobal	7953 82449*	I	2A
38		Honda	7855 82440*	I	2A
39		Marbas Chico Norte (MB)	808170 8244494	II	2A
40		Marbas Chico Sur (CMB)	807408 8243274	II	2A
41		Cerro Pucaguada (CP4)	803335 8241700	II	2B
42		Marbas Grande (MBS)	802111 8244972	II	2A
43		Llajuapampa	807137 8247181	II	2A
44		Uchan Sur	807336 8233573	I	2A
45		Tururunca (H44)	806564 8235286	I	2A

GPS position: * – Smoll et al. (1997); age: * – Cabrera and Thouret (2000); ** – Eash and Sandor (1995)

APPENDIX 3

Major (wt.%) and selected trace (ppm) element contents in samples from Andahua Group rocks

Cluster	A. Valley of the Volcanoes						B. Antapuna		
GPS position	792385 8275084	795273 8259586	–	795735 8289204	790751 8280573	773179 8296462	800840 8335778	783680 8340670	779944 8322476
Sample	AS1	AYO5	MAM3	A14	CH2S	APS4	AR2	PUM1	ANTA2
SiO_2	60.30	61.09	58.61	54.36	57.75	59.78	55.28	57.88	58.88
TiO_2	1.09	1.05	1.21	1.50	1.34	1.21	1.43	1.22	1.22
Al_2O_3	16.19	16.41	16.81	16.98	17.04	16.51	17.09	17.18	16.48
Fe_2O_3	6.44	5.64	6.63	8.01	6.75	5.9	7.56	6.62	6.69
MnO	0.08	0.07	0.08	0.10	0.08	0.07	0.10	0.08	0.09
MgO	3.03	2.35	2.90	4.00	2.85	2.16	3.36	2.71	2.65
CaO	5.28	5.37	5.93	6.92	6.16	4.59	6.50	6.05	5.63
Na_2O	3.99	4.63	4.57	4.80	5.43	4.49	5.16	4.86	4.66
K_2O	2.91	2.90	2.64	1.78	2.52	2.95	2.05	2.63	2.83
P_2O_5	0.39	0.50	0.57	0.54	0.65	0.52	0.61	0.65	0.59
LOI	0.75	0.13	0.49	0.17	0.10	2.41	0.29	1.01	0.82
Total	100.40	100.10	100.40	99.15	100.70	100.5	99.43	100.9	100.5
Rb	77	77	53	29	43	60	33	59	70
Zr	196	186	214	163	219	293	192	224	260
Th	5.6	4.4	2.9	2.1	2.6	4.0	3.3	4.0	6.2
La	45.5	56.6	62	35.7	59.9	47.4	51.5	59.6	59.9
Cr	60	30	40	70	30	20	50	50	40
Ni	–	–	–	40	–	–	30	–	–
$^{87}Sr/^{86}Sr$						0.706187		0.705836	
$^{143}Nd/^{144}Nd$						0.512480		0.512543	

LOI – loss on ignition (Gałaś, 2014, supplemented)

Cluster	C. Rio Molloco Valley		D. Laguna Parihuana	E. Rio Colca Valley				
GPS position	813961 8287058	800936 8335962	195981 8306352	220260 8275352	223066 8275754	224605 8277815	221640 8271073	203782 8269446
Sample	CM	VM21	HT1	OC1	CAN5	CAN1	CAL2	LAR12
SiO_2	67.00	59.60	54.51	59.21	59.78	58.61	57.35	57.41
TiO_2	0.53	1.19	1.51	1.19	1.18	1.21	1.36	0.97
Al_2O_3	14.73	16.65	16.34	16.66	16.76	16.81	16.36	15.82
Fe_2O_3	3.02	5.92	8.11	6.15	6.19	6.63	6.68	5.69
MnO	0.05	0.07	0.11	0.08	0.07	0.08	0.08	0.07
MgO	1.11	2.39	4.32	2.61	2.44	2.90	2.52	2.21
CaO	2.89	5.29	6.81	5.38	5.30	5.93	5.78	5.18
Na_2O	4.40	5.15	4.39	4.64	4.84	4.57	4.74	4.53
K_2O	3.51	2.87	2.09	2.75	3.05	2.64	2.60	2.95
P_2O_5	0.20	0.58	0.63	0.59	0.59	0.57	0.71	0.48
LOI	1.33	0.27	0.52	0.39	0.00	0.49	–0.01	0.18
Total	98.77	99.98	99.35	99.65	100.2	100.40	98.19	95.50
Rb	141	67	38	70	73	58	56	89
Zr	159	253	184	266	234	232	202	194
Th	11.5	4.5	4.4	5.7	5.5	5.4	4.5	10.5
La	35.8	61	45.4	66	76.4	74.7	70.6	58
Cr	–	20	110	30	30	30	30	40
Ni	–	–	50	–	–	–	–	–
$^{87}Sr/^{86}Sr$					0.705965			
$^{143}Nd/^{144}Nd$					0.512501			

Cluster	F. Pampa Jarán						
GPS position	788685 8249704	792926 8243683	807336 8233573	791760 8242573	806254 8247247	802015 8244791	802791 8242138
Sample	GU12	H58	H44	GL8	H010	MBS	CP4
SiO_2	53.51	55.55	52.35	52.13	57.66	55.72	58.89
TiO_2	1.57	1.63	1.40	1.97	1.27	1.43	1.15
Al_2O_3	16.14	16.62	17.2	15.97	16.73	16.71	16.54
Fe_2O_3	7.14	7.37	8.22	9.04	6.38	7.51	5.82
MnO	0.09	0.08	0.11	0.11	0.08	0.09	0.07
MgO	2.84	2.98	3.69	3.91	2.51	3.35	2.34
CaO	6.72	6.46	7.38	7.12	5.52	6.64	5.80
Na_2O	4.84	5.23	4.57	4.01	5.18	4.21	5.06
K_2O	2.45	2.33	2.11	2.02	2.97	1.94	2.94
P_2O_5	0.84	0.80	0.56	1.06	0.66	0.66	0.59
LOI	0.10	0.33	1.40	0.60	0.49	1.30	1.70
Total	96.23	99.38	98.99	97.94	99.44	99.56	100.90
Rb	44	40	25	39	62	34	62
Zr	201	208	223	165	269	185	263
Th	2.4	2.3	3.3	4.3	3.5	2	3.9
La	65.1	60	53.2	71.5	65.9	41.4	62
Cr	30	30	70	70	30	60	20
Ni	–		40	–	–		–
$^{87}Sr/^{86}Sr$				0.705933			
$^{143}Nd/^{144}Nd$				0.512541			

Cluster	G. Huambo-Cabanaconde				
GPS position	811457 8269200	807848 8258375	819574 8262445	816198 8267803	–
Sample	SO8	HU2	MJ3	LE3	KEY1
SiO_2	58.78	55.39	58.69	59.57	56.42
TiO_2	0.99	1.21	1.02	0.98	1.41
Al_2O_3	16.2	16.25	16.46	16.19	17.21
Fe_2O_3	6.20	6.82	7.09	6.24	7.75
MnO	0.10	0.08	0.09	0.09	0.09
MgO	2.78	3.31	3.06	2.98	3.57
CaO	5.40	7.28	5.49	5.73	7.20
Na_2O	3.66	3.27	3.57	3.98	4.04
K_2O	3.34	1.73	2.98	3.29	1.99
P_2O_5	0.34	0.55	0.33	0.32	0.50
LOI	1.00	3.53	1.41	1.38	0.46
Total	98.82	99.43	100.20	100.80	100.70
Rb	92	35	84	89	36
Zr	223	161	225	243	169
Th	10.4	4.2	10.4	9.7	3.8
La	46.7	33.6	51	45.7	35.5
Cr	30	20	40	30	50
Ni	–	–	–	20	–
$^{87}Sr/^{86}Sr$			0.706633		
$^{143}Nd/^{144}Nd$			0.512393		